This is to certify that the

thesis entitled

New Synthetic Methods for Preparation of Cerium Promoted γ-AL_2O_3 Catalysts

presented by

Radu Craciun

has been accepted towards fulfillment
of the requirements for

M.S. degree in Chemistry

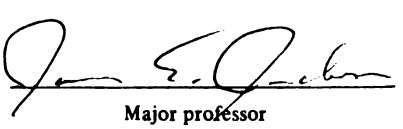

Major professor

Date 9 August 1996

NEW SYNTHETIC METHODS FOR PREPARATION OF CERIUM PROMOTED γ-AL_2O_3 CATALYSTS

By

Radu Craciun

A THESIS

Submitted to
Michigan State University
in partial fulfillment of the requirements
for the degree of

MASTER OF SCIENCE

Department of Chemistry

1996

ABSTRACT

NEW SYNTHETIC METHODS FOR PREPARATION OF CERIUM PROMOTED γ-AL_2O_3 CATALYSTS

By

Radu Craciun

In this study, the structure of CeO_x/γ-Al_2O_3 catalysts have been investigated using diffuse reflectance infrared spectroscopy, X-ray diffraction, and X-ray photoelectron spectroscopy. Fourier transform infrared and ^1H nuclear magnetic resonance spectroscopy have provided information about the structures of various precursors used for impregnation. CeO_2/Al_2O_3 catalysts were prepared by incipient wetness using Ce^{4+} amonium nitrate and by wet impregnation using cerium methoxyethoxide precursor. Different cerium loadings on Al_2O_3 supports have been considered in this study. Impregnation with nitrate solutions occurs with formation of $Ce(OH)_x$ which interacts with the support through hydrogen bonds, whereas the wet impregnation occurs through a grafting process which implies a covalent bond formation between the cerium alkoxide and the surface hydroxyl groups on alumina. After catalyst calcination, the ratio between the crystalline and amorphous CeO_2 on the Al_2O_3 is a function of loading, thermal treatment, and precursor. CeO_2 particle size have increased with the cerium loading and calcination temperature. Surface analysis have indicated that cerium is present as Ce^{4+} on the catalysts surface.

to my father

ACKNOWLEDGMENTS

I would like to thank Dr. Jeffrey Ledford and Dr. James Jackson for their support and guidance during the course of this work and for all the knowledge I obtained in this period of time. I would like to thank Liliana for the understanding me during these years. I would also like to thank the Ledford group members, especially to my friends Paul and Mike, for their help and assistance during the work in the lab, for the past two years.

TABLE OF CONTENTS

LIST OF TABLES

LIST OF FIGURES

INTRODUCTION

A number of previous studies have examined the effects of preparation method, cerium content, and catalyst pretreatment on the structure of Ce/Al_2O_3 catalysts. However, little effort has been devoted to the use of different cerium precursors to control the chemical state and dispersion of the cerium supported on γ-Al_2O_3 catalysts. In this study, the effects of cerium precursor, impregnation methods, and conditioning treatments on the structure of Ce/Al_2O_3 catalysts has been examined using diffuse reflectance infrared Fourier spectroscopy (DRIFTS), X-ray diffraction (XRD) and X-ray photoelectron spectroscopy (XPS). Combined information from these techniques will be used to gain information about the structure of the modified precursors, and the modifications observed in the structure of Ce/Al_2O_3 catalysts. The work focuses on developing new synthetic methods that offer control over the bulk and surface structure of CeO_2 deposited on a γ-alumina support.

CHAPTER 1

INTRODUCTION TO POLLUTION CONTROL CATALYSIS

1.1. Overview of Emission Control Reactions

Even though some catalytic reactions were previoudly known and used for production of different chemicals, e.g. ether from alcohol dehydration, the term "catalysis" was introduced into the scientific chemical language, only in 1835 by Berzelius. He was trying to name and explain some of his observations regarding the influence of different additives to a reaction which led to an increase in its rate. Doberreiner revealed a classic example of the catalysis process in an attempt to produce water from hydrogen and oxygen. He directed a jet of hydrogen at a powdered platinum catalyst. The fine particles instantly became hot and the hydrogen caught fire. This was the scientific principle for the so called "feuerzeug" meaning lighter or tinder box [1,2]. So, total oxidation reactions were among the first chemical transformations performed under heterogeneous catalysis conditions, when platinum played the role of the solid catalyst for the gas phase reaction between H_2 and O_2. From that time, the demand for different chemicals required by the industry and the great technical developments in new analysis techniques and apparatus allowed the introduction of a wide variety of catalysts for total oxidation or combustion reactions.

The great interest in the last years in environmental protection and air pollution control, has necessitated new technology and instruments development. Air pollution causes respiratory illness and other diseases, damage to plants and animals, and other effects on a global scale. Air pollution is defined as any atmospheric condition in which

substances are present at concentration high enough above their normal ambient levels to produce a measurable effect on man, animals, vegetation, or materials. The study of emission sources, such as the internal combustion engine, burning of coal and oil in industrial furnaces, requires a knowledge of the chemistry of combustion as well as of engineering aspects. The secondary products from a chemical process or the *refuse* from different technologies, can be an important factor in pollution. The high cost of burning these materials can play a key role for large investments, which may lead to the development of new low-cost technology for environmental protection. One of the best ways to control air pollution is to prevent contamination from entering the atmosphere. In fact there are three strategies available for reducing the impact of chemicals on the environment: waste minimization, emission abatement, and remediation. Waste minimization calls for the design and development of products and processes that are inherently low polluting or non-polluting. The abatement of emission, considered mostly for air pollution minimization, can often be achieved by trapping harmful effluents or converting them to harmless substances. Remediation is the name given to the use of catalytic processes to clean up contaminated soil or water. This process is potentially the most cost-effective approach, either by using various solid materials or enzymes as catalysts, for contaminant decomposition into harmless compounds.

Unpolluted air is a concept implying a composition of air which would not adversaly affect people's health. The substances usually considered air pollutants are chemicals such as sulfur (SO_x), halogen ($C_3H_xCl_y$), or nitrogen (NO_x) based compounds and radioactive compounds (Rn). Concentrations of air pollutants are measured in ppm

or $\mu g/m^3$. Recent studies have shown that high concentrations of chlorinated hydrocarbons influence the ozone concentration in the stratosphere. Protection of the ozone layer by controlling emissions from chemical industry has been a significant scientific concern. Particular attention has focused on the mechanisms involved in atmospheric ozone formation and consumption due to UV radiation and various other chemicals present in the air [3].

Combustion of waste materials is another way to avoid environmental pollution. Catalytic combustion or incineration as an economical alternative to simple combustion is an important part of modern emission control technology. Interest has therefore developed in the study of the catalytic total oxidation reactions. The main advantages offered by catalytic incineration are the wide range of fuel concentration used in the process and the low temperature at which the reactions can occur compared with the uncatalyzed ones.

Catalytic exhaust gas treatments, especially for automobiles, operate in a temperature range of 600-800°C. The use of total oxidation catalysts for high-temperature processes (>1000°C) became more difficult because catalysts such as supported noble metals or transition metal oxides are not resistant to such conditions. Therefore, it has become necessary to develop new materials which may be used as catalysts or supports for these types of processes. The development of advanced heterogeneous catalysts involves several important activities. These include the development of sophisticated preparation procedures that can be used to design specific

surface structures, guided by examination of the active sites as well as promoters/supports and promoters/transition metal oxides interactions in the active catalytic phases.

At present, the catalyst systems used in these processes are based on noble metals which are expensive and susceptible to poisoning. Transition metal oxide catalysts have been suggested as suitable substitutes for noble metals even though they are not as active and are also subject to poisoning. The advantages of transition metal oxides are their low cost and better resistance to chlorine poisoning. By improving their stability, selectivity and activity using suitable promoters, transition metal oxides may become good replacements for noble metal-based catalysts.

In thermal combustion (1500-2000°C), gas-phase radicals are initiated thermally after which oxidation reactions occur rapidly. At high temperature nitrogen oxides are formed from nitrogen and oxygen in the air. The presence of these nitrates oxides in exhaust gases is undesirable from a pollution control point of view. Control of the reaction at these high temperatures is very difficult due to the limited flexibility in the fuel concentration. These difficulties challenge science to develop new catalytic processes which can avoid the inconvenience of thermal incineration.

The mechanisms involved in catalytic incineration are complex and a better understanding of the processes which take place on the catalyst surface would be desirable. Prasad *et al.* [3] summarized some of the properties for suitable catalysts used in catalytic incineration processes. Among these can be mentioned a low ignition temperature of the fuel/air mixture, high catalytic activity and durability over time, resistance to high temperature and mechanical shocks, and suitable supports with high

surface area. There are a few classes of materials which approach all these requirements, but none that fulfilled all.

Noble Metals. Catalytic incineration over noble metal catalysts has been widely used for decades. The advantages of these catalysts are given by the high catalytic activity and selectivity. Platinum, palladium and rhodium are the most commonly used active phases for catalytic combustion applications [4-6]. A desirable characteristic of the noble metal catalysts is their high resistance to sulfur poisoning compared with the transition metal oxide catalysts [7]. Highly dispersed Pt and Pd catalysts are easily prepared using a number of support materials like silica or alumina.

Oxidation over noble metals is considered to be a structure sensitive reaction which means that the surface configuration of the catalyst will strongly influences the activity, selectivity, reaction pathway and the rate [8-12]. Briot *et al.* [8-9] have attributed the activity of supported platinum and palladium catalysts to the high specificity of surface oxygen on large crystallites. For these type of catalysts, an activity enhancement was observed at low temperature, close to the catalyst ignition temperature. Catalysts with high noble metal dispersion (small crystallites) exhibit high catalytic activity [10]. No oxygen pressure dependence on the reaction rate was found. In the case of methane oxidation, the reaction order was found to be around one in methane with little influence of oxygen concentration on the reaction rate. The dissociation of the methane or oxygen-methane complexes at the catalyst surface was proposed to be the rate-limiting step in the mechanism [12].

Transition Metal Oxides. Oxidation over solid metal oxide catalysts has been widely studied during the last years. The main advantage over noble metal catalysts is

the low cost of the raw material. By choosing a well defined composition of the metal oxide in the catalyst, an oxidation activity close to that of the noble metal catalysts can be obtained. It was found that the formation of nitrogen oxides can be avoided using metal oxide catalysts [13]. Oxygen can be activated by interaction with the catalyst surface.

Coordination or incorporation into the oxide lattice may be an important step in catalyst activation. Lattice incorporation leads to a more strongly bound oxygen than in the case of simple physical adsorption. The lattice oxygen was found to be more active in the case of selective oxidation processes whereas the surface oxygen was more important in complete oxidation reactions [14]. Participation of lattice oxygen in complete oxidation reactions increases with temperature. Wise *et al.* [15] observed that the ratio of the rate constants corresponding to the reactions of lattice oxygen and adsorbed oxygen increases with temperature from 0 at 500°C to 0.3 at 800°C for methane oxidation on a $LaFeO_3$ catalyst. At higher temperatures lattice oxygen interactions dominate the oxidation process. Many studies have been focused on the suitability of different types of metal oxides for catalytic incineration, trying to rationalize their catalytic activity. Comparison studies of the catalytic activities in terms of conversion for a variety of oxides such as Cr_2O_3, Co_2O_3 [16], Mn_2O_3 [17] V_2O_5 [18], or CuO [19] led to the conclusion that many of these oxides are potentially good catalysts for total oxidations.

Mixed oxides with perovskite structures XYO_3, (where X and Y are different transition metals), revealed high activity in total oxidation reaction [20]. The use of perovskite-type oxides as catalysts was first reported in 1970, by Meadowcroft [21]. Their well defined and stable structure make them suitable for oxidation catalysts.

Perovskite electronic structures are comparable with those of the transition metals. Seiyama [20] summarized in a review article the important aspects of total catalytic oxidation reaction on various perovskite oxides, like sorption and desorption of oxygen, H_2 oxidation and total oxidation of hydrocarbons. Many of the pervoskite structures incorporated lanthanides (La, Ce, Pr) and/or alkaline earth metals (Ba, Sr, Ca) in combination with transition or noble metals. Structures like $La_{1-x}Sr_xBO_3$, $La_{1-x}Sr_xMnO_3$, $La_{1-x}Sr_xCoO_3$ [22-24] are some of the most recent perovskite-type catalysts prepared and used successfully in total oxidation reactions.

From the material presented above we can conclude that a great number of high-temperature-stable complex oxide materials are promising catalysts for catalytic incineration.

Supports. Another important element in the structure and composition of catalyst is the support. The chemical nature of these may play an important role in the catalyst activity. Supports are mostly used to improve thermal and chemical stability while decreasing the amount of the expensive active component required to make a catalyst. The surface area and chemical nature of the support play major roles in the behavior of the catalysts. The most often used supports are based on silicates and aluminates, but often less resistant, low surface area materials with low surface area such as MgO or TiO_2, are used to improve the selectivity of a catalyst or as a catalyst site itself. The geometry and the dimension of the particle used as support are very important factors in the catalyst activity. The characteristics needed for a support to be used in high-temperature reactions such as combustion can be summarized as follows: i) high thermal stability and mechanical strength; ii) no chemical reaction between support and the

catalytic component; iii) high volume throughput [25]. It is hard to find an ideal material that meets all the requirements for an excellent support. Many times, additives or promoters are used to improve the properties of the supports used for catalyst preparation. Silica is one of the most commonly used support materials; at high temperature and in the presence of oxygen, silica exhibits sintering phenomena. γ-Al_2O_3 is another support that shows resistance to the sintering process compared to silica. However, at very high temperature (1000°C) the γ-Al_2O_3 phase is transformed into α-Al_2O_3 which has a lower surface area [26]. Many studies on alumina based catalysts show loss in surface area due to sintering of particles by solid-state diffusion. Consequently, the thermal treatment used for the support material also affects a catalyst's properties [27].

As was previously mentioned, addition of promoter may stabilize the support inhibiting the sintering process. Promoters can be divided in two different classes: structural and textural. Structural promoters will lead to a transformation of the catalysts surface configuration which will affect the catalyst activity. Textural promoters will have less influence on the structure of the catalyst but will improve the textural properties of the catalyst like surface area, pore volume size, and mechanical resistance of the catalyst surface. Alkali earth metals (Ba, Ca, Sr) are well known as additives with consequence on the textural properties as well as mechanical resistance of the catalysts. Lanthanide oxides are known to be used as both textural and structural promoters, influencing the thermal resistance and the surface configuration of the catalyst. Another way to promoter a catalyst is to introduce lattice flaws into the structure. These kind of promoters were called electronic promoters, substances with semiconductor character.

These materials will accept or lose electrons from conduction band. Impurities in the lattice of the catalyst will determine an increase its catalytic activity.

1.2. Rare Earth Promoters used in Different Oxidation Reaction

As was described before, catalysis has become an important field of study for environmental pollution control processes. Dispersion of the active component, loading and surface structure are important parameters in designing a proper catalyst. The main chemical effect of a catalyst in total oxidation reactions is to force them to completion, yielding water, carbon dioxide and nitrogen as final products (assuming only C, O, H, N are in the feed). Another important effect is a decrease in the incineration temperature.

Metal oxide based catalysts are of particular interest for these types of processes. Procedures such as temperature treatment, or additives such as promoters or activators may strongly influence the surface structure of the catalyst and its catalytic activity. Manipulation of these factors during catalyst preparation offers control over activity, selectivity and resistance of the catalyst to various poisons or inhibitors. Tailoring a catalyst surface by controlling the dispersion and/or particle size of the active phase, crystalline structure and oxidation state of the metals on the surface, ultimately gives control over the catalytic process.

Promoter effect. Rare earth additives have been employed extensively as textural and structural promoters in supported metal catalysts [28-30]. Cerium oxide in particular has been widely used for these purposes [31-39]; its promoter effect is given by the nonstoichiometrical crystal structure [40-41], oxygen storage capabilities [42-45], redox properties [46] and very good thermal resistance [47-53]. Cerium promotion enhances

the catalytic activity of transition metals and/or transition metal oxides supported catalysts for CO oxidation and NO_x reduction because of its ability to form oxygen-deficient oxides under reducing conditions [49,40]. Due to their importance in a variety of catalytic applications, the structures of supported cerium catalysts have been the focus of many investigations [29-59]. Miki *et al.* [42] have used XRD to examine the structure of a 20 wt.% CeO_2/Al_2O_3 catalyst oxidized and reduced at high temperature (900°C). High temperature reduction of the catalysts led to the $CeAlO_3$. Reoxidation of the reduced catalysts had no effect on $LaAlO_3$ whereas $CeAlO_3$ was reoxydized to CeO_2. Shyu *et al.* [57] reported XPS, Raman spectroscopy, and TPR results for a series of Ce/Al_2O_3 catalysts. They concluded that Ce existed as a $CeAlO_3$ precursor, small CeO_2 crystallites, and large CeO_2 particles on Ce/Al_2O_3 catalysts. Recently, Graham *et al.* [35] reported that lanthanum promotion increases the dispersion and the range of reversible reducibility of alumina supported CeO_2.

Spectroscopic measurements combined with *ab initio* calculations have shown that in the case of supported rare earth oxides on alumina, modification of the electronic structure of the lanthanide cation occurs affecting the catalytic properties of the catalyst. Charge redistribution over an alumina surface implies a modification of the acid-base characteristic of the active sites [60]. Lanthanide cations are known to have strong interaction with the support which results in an electronic density redistribution. Metal-support interactions influence both the electronic state of the metal and the surface morphology. The Al_2O_3 support provides a weak ligand field, favoring the high-spin state of the metal and a change in the oxidation state [61].

The crystallographic and solid-state properties of the lanthanide oxides can be largely limited to the so-called sesquioxide stoichiometry (M_2O_3), the only stable composition ordinarily observed for these materials. Exceptions from this structure have been observed in the cases of EuO_x and SmO_x. Dioxides having a face-centered cubic structure (fluorite type structure), are known in the case of Ce, Pm and Tb but only the cerium stoichiometry is more stable than the corresponding sesquioxide structure, mostly due to the stability of the Ce^{4+} oxidation state. Ce_2O_3 can be prepared only with difficulty, by extended reduction of CeO_2 at high temperature or by vacuum decomposition of certain salts. Ce_2O_3 oxidizes easily in air to the dioxide. In addition, the oxide system of Ce and Tb contain well-defined composition of LnO_x ($1.5 < x < 2.0$). In all three systems mentioned above as characteristic for lanthanides oxides, the stable phases shows variable Ln^{3+}/Ln^{4+} ratios together with the appropriate number of O^{2-} ions needed to achieve electrical neutrality. Rare earth sesquioxides exhibit characteristic polymorphism and can exist in one or more distinct crystalline modifications, depending on the radius of the tetravalent metal ion and the temperature for oxide preparation and quenching. Pertinent parameters of the rare earth cations and stable rare earth oxide phases are available in literature [62]. X-ray diffraction patterns of most of these materials are also available for comparative purposes [63]. Various oxide modifications may be further distinguished by bond differences that occur in the 200-700 cm^{-1}, in the IR-spectral region. All anhydrous rare earth oxides are ≈75% ionic having a good basic character (important property in catalytic purpose).

Lanthanide oxides undergo dehydration/rehydration processes. This cyclic process was used to prepare Ln_2O_3 having highly reproducible catalytic activities for alcohol dehydrogenation/dehydration and for double bond isomerizations of olefins [64]. For some reactions, catalytic activities are independent of electronic or magnetic properties of the oxides and is determined by relative acid-base properties or by the surface structure of the catalysts whereas for other types of reactions paramagnetic nature, lattice oxygen mobility and cation variable valence play important roles, governing the catalytic behavior. For instance, the paramagnetic rare earth oxides have been shown in several studies to be effective catalysts for ortho-para hydrogen conversion [65]. The rate is strongly influenced by the temperature which affects the paramagnetic properties of the catalyst materials. Diamagnetic oxides such as Y_2O_3 or Lu_2O_3 can be activated by thermal treatment which apparently generates the paramagnetic ions Y^{2+} and Lu^{2+} [66].

Preparation methods. The precursors and/or methods used for preparation can strongly influence the surface structure of a catalyst and consequently its catalytic activity and selectivity. The most widely used precursor for cerium impregnation utilized often for preparation of three way catalysts for automotive exhaust systems, is the Ce^{3+}-nitrate solution [67]. After calcination, a well dispersed cerium phase is observed on the Al_2O_3 support, at low cerium loading [67-68]. Miki *et al.* [42] prepared a cerium catalyst by incepient wetness impregnation and compared its surface structure with a cerium catalyst prepared by the sol-gel technique, which uses Ce^{3+}-nitrate dissolved in ethylene glycol and aluminum tri-isopropoxide. Different CeO_x surface structures were obtained which led to modified catalytic behavior.

Ion exchange is an alternative method used for preparation of catalysts [69, 70]. The method is based on the electrostatic adsorption of the ions at a pH lower than the isoelectric point (IEP) characteristic for each support when the surface is positively charged and anion adsorption can occur. Positive and negative charged support surfaces can adsorb positive or negative charged ions from the solution. The exact chemistry depends on support, pH and species in solution. The pH value of the solution will act as a surface charge selection switch, favoring the deposition of a given ion. Using this method, molybdenum was successfully well dispersed on TiO_2 [71] and Al_2O_3 [72] supports. Difficulties in controlling the equilibrium of ionic species present in the precursor solutions at various pH values preclude the general utilization of this technique.

For metal impregnation, Kummer *et al.* [73] proposed a method which involves thermal transport from bulk phase of a metal foil to a dispersed phase on the support surface. The metal concentration on such catalysts is low but highly dispersed. In this way, cerium was deposited on the support by incipient wetness impregnation using Ce^{3+}-nitrate solution, before the transition metal impregnation. Such catalysts used CeO_2 as an additive favoring the metal transport (in this case, Pt) and dispersion, leading to a very complex CeO_2-metal surface structure.

Dufour *et al.* [74] used organometallic compounds for rhodium impregnation of a silica support. The interaction mode of the $Rh(\eta^3\text{-}C_3H_5)$ with the oxide support varies according to the nature and the degree of hydroxylation of the support. Different grafted rhodium species were found on the support surface after impregnation. Didillon *et al.* [75] extended the use of organometallics for other transition metals (group VIII-metals)

and found that highly dispersed metal phases can be successfully anchored onto low-surface area Al_2O_3. Usmen *et al.* [76] used a La^{3+} pretreated alumina as a support to form a well dispersed cerium phase during impregnation. They found that well dispersed La^{3+}-phases interact with CeO_2 leading to a better cerium and platinum dispersion. Higher cerium dispersion leads to the retention of more reducible oxides such as $CeAlO_3$ with consequences on the oxygen storage capacity of the catalyst [57].

Van Hengstum *et al.* [77] and later Baiker *et al.* [18] have developed a synthetic method for catalyst preparation that involves alkoxide grafting using a metal-organic compound. Generally, an alkoxide grafting reaction may be written as follows:

$$\text{Support-OH} + \text{M-(OR)}_x \rightarrow \text{Support-O-M(OR)}_{x-1} + \text{R-OH} \qquad (1\text{-}1)$$

The chemistry of this method involves the formation of a covalent bond between the metal center and the support surface, followed by the elimination of an alkoxide ligand from the metal center (M) as an alcohol. Excellent dispersion was obtained for vanadium impregnation on different supports (SiO_2, Al_2O_3 or TiO_2), when vanadium tert-isobutyl solution was used as a precursor.

For example, silica-supported ceria catalysts of various content (less than 11% Ce) were prepared by anchoring cerium acetylacetonate in organic media and studied their surface strucuture. The resulting CeO_2 particles were 1-3 nm diameter after calcination in oxygen at 673 K. The highly dispersed ceria obtained by using the cerium acetylacetonate precursor shows a shift to higher XPS binding energies for Ce3d and O1s, increased CO stretching in CO-Ce^{4+} terminal groups, and a blue shift of the band gap measured by diffuse reflectance in comparison with catalysts prepared using the classical preparation by incipient wetness using cerium nitrate [78].

The use of a "hot grafting" technique refers to a grafting process using a metal-alkoxide precursor under reflux condition and elevated temperature. This technique can be an alternative way to improve the interaction between the precursor and support surface [79]. The high cost as well as the sensitivity to air and water of these metal-organic compounds [80], confer to the grafting method a disadvantage for large scale catalysts impregnation. It was found that in some cases, the presence of ethanol in the system as an exchange ligand influences the reactivity of cerium alkoxide toward grafting with the hydroxyl groups from the support surface [81].

Recently, lanthanide alkoxide catalysts were successfully used in some organic reactions like synthesis of vitamins and steroids [82, 83], being promising catalysts for heterogeneous catalysis processes applied in organic synthesis. If these alkoxides are prepared from chiral alcohols, the catalysts obtained may be used to perform asymmetric synthesis, largely applied in the drug industry [84]. A monolayer dispersion of the impregnated lanthanide-alkoxide, fixed on a solid support, may confer on the catalysts increased selectivity and activity in these types of organic synthesis.

1.3 References

1. Collins, P. *Ambix*, **1976**, *23*, 96.
2. Thomas, J. M. *Angew. Chem. Int. Ed. Engl.* **1994**, *33*, 913-937.
3. Prasad, R.; Kennedy, L. A.; Ruckenstein, E. *Catal. Rev. - Sci. Eng.* **1984**, *26(1)*, 1-58.
4. Hicks, R. F. *Chem. Eng. Sci.* **1990**, *45(3)*, 2647-2651.
5. Worley, S. D.; Rice, C. A.; Mattson, G. A.; Curtis, C. W.; Guin, J. A. *J. Chem. Phys.* **1982**, *76*, 20-24.
6. Taylor, K. C. in *Catalysis and Automotive Pollution Control* by Crucq, A.; Fressnet, A. **1987**, Elsevier, Amsterdam.
7. Johnson, D. W. Jr. *J. Catal.* **1977**, *48*, 87-97.
8. Briot, P. *Appl. Catal.* **1990**, *59*, 141-152.

9. Briot, P.; Primet, M. *Appl. Catal. 1991, 68*, 301-314.
10. Hick, R. F. *J. Catal.* **1990**, *122*, 295-306.
11. Baldwin, T. R.; Burch, R. *Appl. Catal.* **1990**, *66*, 359-381.
12. Otto, K. *Langmuir*, **1989**, *5*, 1364-1369.
13. Ismagilov, Z. R.; Kerzhentsev, M. A. *Catal. Rev.-Sci. Eng.* **1990**, *32(1,2)*, 51-103.
14. Arakawa, T.; Tsuchi, Y. S.; Shiokawa, J. *J. Catal.* **1982**, *74*, 317-322.
15. Wise, H.; McCarty, J. G. *Catal. Today*, **1990**, *8*, 231-248.
16. Prasad, R.; Kennedy, L. A.; Ruckenstein, E. *Combust. Sci. Technol.* **1980**, *22*, 271-275.
17. Dwyer, F. G. *Catal. Rev.* **1972**, *6(2)*, 261.
18. Kifenski, J.; Baiker, A.; Glinski, M.; Dollenmeier, P.; Wokaun, A. *J. Catal.* **1986**, *101*, 1-11.
19. Lu, G.; Wang, R. *Cuilua Xuabao*, **1991**, *12(4)*, 261-267 (Ch).
20. Seiyama, T. *Catal. Rev. - Sci. Eng.* **1992**, *34(4)*, 281-300.
21. Meadowcroft, D. B. *Nature*, **1970**, *226*, 847.
22. Jaecnicke, S.; Chuah, G. K. *Ber. Bunsenges. Phys. Chem.* **1992**, *96(1)*, 1-9.
23. Arai, H. *Appl. Catal.* **1986**, *26*, 265-276.
24. Zhang, H. M.; Teraoka, Y.; Yamazoe, N. *Appl. Catal.* **1989**, *6(1,2)*, 155-162.
25. Zwinkels, M. F. M.; Jaras, S. G.; Menon, P. G.; Griffin, T. A. *Catal. Rev. - Sci. Eng.* **1993**, *35(3)*, 319-358
26. Beguin, B.; Garbowski, E.; Primet, M. *J. Catal.* **1991**, *127*, 595-604.
27. Tijburg, I. I. M.; Geus, J. W.; Zandbergen, H. W. *J. Mater. Sci.* **1991**, *26*, 6479-6486.
28. Alvero, R.; Bernal, A.; Carrizosa, I.; Odriozola, J. A. *Inorg. Chim. Acta*, **1987**, *140*, 45-48.
29. Xie, Y. C.; Qian, M. X.; Tang, Y. Q. *China-Japan-U.S. Symposium on Heterogenous Catalysis Related to Energy Problem*, **1982**, *B.10C*,China.
30. Yang, J. Y.; Swartz, W. E. *Spectrosc. Lett.* **1984**, *17*, 331-332.
31. Baiker, B. G.; Clark, N. J. in *Studies in Surface Science and Catalysis*, Delmon, B. Grange, P. Jacobs, P. A. Poncelet, G. Elsevier, Amsterdam, **1987**, *31*, 455-62.
32. Kieffer, R.; Kiennemann, A.; Rodriquez, M.; Bernal, S.; Rodriquez-Izquierdo, J. M. *Appl. Catal.* **1988**, *42*, 77-86.
33. Shyu, J. Z.; Otto, K.; Watkins, W. L. H.; Graham, G. W.; Belitz, R. K.; Gandhi, H. S. *J. Catal.*, **1988**, *114*, 23-28.
34. Hay, C. M.; Jennings, J. R.; Lambert, R. M.; Nix, R. M.; Owen, G.; Rayment, T. *Appl. Catal.* **1988**, *37*, 291-304.
35. Graham, G. W.; Schmitz, P. J.; Usmen, R. K.; McCabe, R. W. *Cat. Lett.* **1993**, *17*, 175-184.
36. Masuda, K.; Kawai, M.; Kuna, K.; Kachi, N.; Mizukami, F. in *Preparation of Catalysts V Ed.* Poncelet, G.; Jacobs, P. A.; Grange, P.; Delmon, B.; Elsevier, Amsterdam, **1991**, 229-238.
37. Sugiyama, S.; Matsumura, Y.; Moffat, J. B. *J. Catal.* **1993**, *139*, 338-350.
38. Ledford, J. S. *Ph. D. Thesis*, University of Pittsburgh, **1989**.
39 Dulamita, N. *Rev. Rom. Chim.* **1985**, *36(11)*, 1050.
40. Steinberg, M. *Anal. Appl. Rare Earth Mater. Nato Adv. Study Inst.* **1972**, 263-270.

41. Perrichon, V.; Laachir, A.; Bergeret, G.; Frety, R.; Tournayan, L.; Touret, O.; *J. Chem. Soc. Faraday Trans.* **1994**, *90(5)*, 773-781.
42. Miki, T.; Ogawa, T.; Haneda, M.; Kakuta, N.; Ueno, A.; Tateishi, S.; Matsuura, S.; Sato, M. *J. Chem. Phys.* **1990**, *94*, 6464-6467.
43. Yao, H. C.; Yao yu, Y. F. *J. Catal.* **1984**, *86*, 254-265.
44. Su, E. C.; Montreuil, C. N.; Rothschild, W. G. *Appl. Catal.* **1985**, *17*, 75-86.
45. Loof, P.; Kasemo, B.; Keck, K. E. *J. Catal. 1989, 118*, 339-348.
46. Haneda, M.; Mizushima, T.; Kakuta, N.; Ueno, A.; Sato, Y.; Matsuura, S.; Kasahara, K.; Sato, M. *Bull. Chem. Soc. Jpn.* **1993**, *66*, 1279-1288.
47. Schaper, H.; Doesburg, E. B. M.; VanReijen, L. L. *Appl. Catal.* **1983**, *7*, 211-220.
48. Pembo, J.M.; Lenzi, M.; Lenzi, J.; Lebugle, A. *Surf. Inter. Anal.* **1990**, *15(11)*, 663.
49. Yu-Yao, Y.F.; Kummer, J.T. *J. Catal.* **1987**, *106*, 307.
50. Chojnacki, T.; Krause, K.; Schmidt, L.D. *J. Catal.* **1991**, *128(1)*, 161.
51. Oudet, F.; Courtine, P.; Vejux, A.J. *J. Catal.* **1988**, *114*, 112.
52. Yang, J.K.; Swartz, W.E. *Spectrosc. Lett.* **1984**, *17(6&7)*, 331.
53. Gaugin, R.; Graulier, M.; Papee, D. *Adv. Chem. Ser.* **1975**, *143*, 147.
54. Koberstein, E. *Unst. St. Proc. Catal.*, Matros, Y.S., Ed., **1990**, 643.
55. Yamaguchi, T.; Ikeda, N.; Hattony, H.; Tanabe, K. *J. Catal.* **1981**, *67*, 324.
56. Raen, S.; Braten, N.A.; Grepstad, J.K.; Qui, S.L. *Phys. Scr.* **1990**, *41(6)*, 1001.
57. Shyu, J. Z.; Weber, W. H.; Gandhi, H. S. *J. Phys. Chem.* **1988**, *92*, 4964.
58. Ledford, J. S.; Houalla, M.; Proctor, A.; Hercules, D. M. *J. Phys. Chem.* **1989**, *93*, 6770-6777.
59. Dulamita, N.; Pop, A.; Corbeanu, V. *Studia*, **1984**, *29*, 3-11.
60. Capitan, M. J.; Centeno, M. A.; Malet, P.; Carrizosa, I.; Odriozola, J. A. *J. Phys. Chem.* **1995**, *99*, 4655-4660.
61. Tauster, S. J.; Fung, S. C.; Garten, R. L. *J. Am. Chem. Soc.* **1978**, *100*, 170.
62. Korner, R.; Ricken, M.; Nolting, J. *J. Solid State Chem.* **1989**, *78*, 136-147.
63. *Powder Diffraction File*, Inorganic Phases, JCPDS, **1983**.
64. Rosynek, M. P.; *Cat. Rev. - Sci. Eng.* **1977**, *16(1)*, 111-154.
65. Baron, K.; Selwood, P. W. *J. Catal.* **1973**, *28*, 422-426.
66. Aries, J. A.; Selwood, P. W. *J. Catal.* **1974**, *33*, 284-288.
67. Kubsh, J. E.; Rieck, J. S.; Spencer, N. D. in *Catalysis and Automotive Pollution Control II,* ed. Crucq, A. Elsevier, Amsterdam, **1991**, 125-138.
68. Diwell, A. F.; Rajaram, R. R.; Shaw, H. A.; Truex, T. J. *in Catalysis and Automotive Pollution Control II*, ed. Crucq, A. Elsevier, Amsterdam, **1991**, 139-152.
69. Burch, R.; Flambard, A. R. in *Preparation of Catalysts III* by Poncelet, G.; Grange, P.; Jacobs, P. A. Els. Sci. Publ. Amsterdam, **1983**, 311-320.
70. Brunelle, J. P. *Pure Appl. Chem.*, **1978**, *50(9,10)*, 1211-1229.
71. Luthra, N. P.; Cheng, W. C. *J. Catal.* **1987**, *107*, 154-160.
72. VanVeen, J. A. R.; deWitt, H.; Emeis, C. A.; Hendriks, P. A. J. M. *J. Catal.* **1987**, *107*, 579-582.
73. Kummer, J. T.; Yu-Yao, Y. F. *J. Catal.* **1987**, *106*, 307-312.
74. Dufour, P.; Houtman, C.; Santini, C. C.; Basset, J. M.; Hsu, L. Y.; Shore, S. G.

J. Am. Chem. Soc. **1992,** *114*, 4248-4257.

75. Didillon, B.; El Mansour, A.; Candy, J. P.; Basset, J. M.; Le Peltier, F.; Bournonville, J. P. in *Preparation of Catalysts V* ed. Poncelet, G.; Jacobs, P. A.; Grange, P.; Delmon, B. Elsevier, Amsterdam, **1991**, 717-723.
76. Usmen, R. K.; Graham, G. W.; Watkins, W. L. H.; McCabe, R. W. *Catal. Lett.* **1995**, *30*, 53-63.
77. Van Hengstum, A. J.; Van Ommen, J. G.; Bosch, H.; Gellings, P. J. *Appl. Catal.* **1983**, *5*, 207-217.
78. Bensalem, A.; Bozon-Verduraz, F.; Delamar, M.; Bugli, G. *Appl. Catal.* **1995**, *121*, 81-93.
79. Smith, P. D.; Klendworth, D. D.; McDaniel, M. P. *J. Catal.* **1987**, *105*, 187-193.
80. Namy, J. L.; Souppe, J.; Kagan, H. B. *J. Org. Chem.* **1984**, *49*, 2045-2049.
81. Mehrotra, R. C.; Kapoor, P. N.; Botsoara, J. M. *Coord. Chem. Rev.* **1980**, *31*, 67-91.
82. Kirk, D. N.; Slade, C. J. *J. Chem. Soc. Perkin Trans*, **1980,** 1, 2591-2569.
83. Evans, D. A.; Hoveyda, A. H, *J. Am. Chem. Soc.* **1990**, *112*, 6447-6449.
84. LeBrun, A.; Namy, J. L.; Kagan, H. B. *Tetrahedron Letters*, **1991**, *32(21)*, 2355-2358.

CHAPTER 2

NEW SYNTHETIC METHODS FOR PREPARATION OF CERIUM PROMOTED γ-AL_2O_3 CATALYSTS

2.1 Introduction

Cerium oxide has been employed extensively as a textural and structural promoter for supported metal catalysts. The structural promotion effect was attributed to the formation of new active sites (crystallites or structural defects) formed by CeO_x species on the catalyst surface [1-5]. The textural promotion effect is given by the excellent thermal and mechanical resistance conferred on the promoted catalyst. Detailed studies were done to investigate the correlation between catalyst structure and activity. Due to its many catalytic applications, the structure of supported cerium oxide has been the focus of many investigations [6-18]. CeO_2/γ-Al_2O_3 catalysts are commonly used in automotive catalytic converters and for selective or total oxidation reactions. Cerium promotion enhances the catalytic activity for CO oxidation mostly due to its ability to form oxygen-deficient oxides under reducing conditions [8]. In discussing the effects of cerium promoters in three-way catalysts, Nuna *et al.* [17] concluded that a decrease in the CeO_2 crystallites and increase in cerium content led to an increase in catalytic activity and thermal durability. The improvement in catalyst activity have been attributed to the ability of CeO_2 to fix platinum (or Pd) on the catalyst's surface [19-27].

The structure of a CeO_x/Al_2O_3 system is strongly dependent on: i) preparation method (impregnation techniques), ii) the chemical nature of the precursors used for preparation, and iii) temperature treatment during catalyst preparation and iiii) cerium

loading [10-22]. Le Normand *et al.* [20] examined a series of CeO_2/Al_2O_3 and Pd-CeO_2/Al_2O_3 catalysts supported on γ-Al_2O_3 using X-ray photoelectron spectroscopy (XPS) and X-ray absorption spectroscopy (XAS). They found a clear correlation between the cerium loading and its surface structure. For cerium loading below 1.5 wt%, these authors reported that cerium exists as Ce^{3+} cations in octahedral coordinated sites on the Al_2O_3 surface. For higher cerium loading, XPS and XAS data indicated the formation of three-dimensional cerium oxides. Cerium loading has an effect on the stability and dispersion of the Pd deposited on the alumina support, as well. Shyu *et al.* [21] reported XPS, Raman spectroscopy, and temperature-programmed reduction (TPR) results for a series of Ce/Al_2O_3 catalysts. They concluded that Ce existed as a $CeAlO_3$ precursor, small CeO_2 crystallites, and large CeO_2 particles on Ce/Al_2O_3 catalysts. Miki *et al.* [22] used XRD to examine the structure of a 20 wt% CeO_2/Al_2O_3 catalyst oxidized and reduced at high temperature (900°C). High temperature reduction of the catalysts lead to the formation of $CeAlO_3$. Reoxidation of the reduced catalysts had no effect on the $LaAlO_3$ whereas $CeAlO_3$ was reoxidized to CeO_2.

Previous literature data enphasized that a key factor to consider in the study of CeO_2/Al_2O_3 catalyst system is cerium dispersion. Several approaches can be considered in order to improve cerium dispersion. One is the use of efficient impregnation techniques that optimize promoter dispersion on the high surface area support. Pre-impregnation of the support with elements which may favor the cerium dispersion further improve the cerium oxide dispersion. Another approach is to change the chemical nature of the precursor solution used for support impregnation to optimize the interaction

with the support surface and to avoid as much as possible side reactions (*e.g.* precipitation or self polymerization) which may affect the promoter dispersion.

This study is focused on the investigation of chemical interactions and structural transformations of CeO_x species supported on a γ-Al_2O_3 support when various impregnation techniques and thermal treatments were used for catalyst preparation. The interaction between the support and cerium promoter will be investigated using diffuse reflectance infrared Fourier transform spectroscopy (DRIFTS). The effect of cerium loading and thermal treatment on the dispersion of CeO_2 in a series of γ-Al_2O_3 promoted catalysts have been examined using X-ray diffraction (XRD). The oxidation state of supported CeO_x has been investigated using XPS. Information derived from the surface and bulk characterization techniques has been used to establish the effects of cerium precursor and preparation method on the structure of the CeO_2/γ-Al_2O_3 catalysts.

2.2 Experimental

Catalyst Preparation. Catalysts were prepared by impregnation of γ-alumina (American Cyanamid, γ-Al_2O_3, surface area = 200m^2/g, pore = 0.6 mL/g) using various cerium precursors. The alumina support was finely ground (<230 mesh) and calcined in air at 500°C for 24 h prior to impregnation. Catalysts derived from cerium nitrate used water solution of Ce^{4+}-ammonium nitrate precursor (Mallinckrodt Co.) and Ce^{3+}-nitrate 99.9% hexahydrate (Aldrich Co.). Catalysts obtained from cerium alkoxide used Ce^{4+}-methoxyethoxide 18-20% in methoxyethanol (Gelest Co.) as precursor. The cerium content was varied from yx10^{-2}= 0.0x10^{-2} to 8.0x10^{-2}, where y is the Ce/Al atomic ratio

(or from 0 to 22 wt% CeO_2). The catalysts for this study were obtained i) by incipient wetness impregnation, using Ce^{3+}-nitrate (designated "Ce*y*NR") and Ce^{4+}-ammonium nitrate (designated "Ce*y*N"), ii) by wet grafting impregnation using the Ce^{4+}-methoxyethoxide solution. Grafting impregnation was performed under inert atmosphere and continuous mixing, for 48 h. Two different grafting approaches were used: a) "simple grafting" at room temperature without any additives (designated "Ce*y*A") and b) "hot grafting" when the impregnation was carried out at 80-85°C under reflux (designated "Ce*y*HG"), in the presence of ethanol. All samples were dried at 120°C for 16 h and calcined at 500°C and 800°C, respectively. In order to follow the transformations that take place during the thermal treatment, the Ce8-samples were calcined at 200°C and 300°C and analyzed. The actual cerium concentrations in the catalysts were determined by inductively coupled plasma (ICP) analysis, the results showing an estimated error of ± 10% in comparison with those theoretically calculated and added during preparation.

Standard Materials. CeO_2 was prepared by calcining Ce^{4+}-ammonium nitrate (Aldrich Chemical Company) at 500°C for 16 h. XRD patterns of the standard compounds matched the appropriate Powder Diffraction File [28].

BET Surface Area. Surface area measurements were performed using a Quanta-Chrome Quantasorb Jr. Sorption System. Approximately 0.1 grams of catalyst were outgassed in N_2 at 165°C for 12h prior to adsorption measurements. The measurements were made using relative pressures of N_2 to He of 0.05, 0.08, and 0.15 (N_2 surface area = 0.162 nm^2) at 77 K. The estimated error for the surface area measurement is ± 5%.

Diffuse Reflectance. Diffuse reflectance spectra were acquired using a Mattson-Galaxy FTIR-3020 instrument with a diffuse reflectance attachment from Spectra-Tech Inc. The catalyst powders (20-25 mg) were put into the sample holder, introduced into the DRIFTS attachment. The IR beam is focused using an ellipsoidal mirror from the attachment, diffuses into the powder, where it undergoes reflection, refraction, diffusion and absorption before reemerging at the surface. After the beam is collected from the sample using the same ellipsoidal mirrors, is focused onto the IR detector and analyzed. The spectra collected are in Kubelka-Munk units versus wavenumber [29]. IR spectra were acquired with resolution of 2.0 cm^{-1} over a 400-4000 cm^{-1} wavenumber range.

X-Ray Diffraction. X-ray powder diffraction patterns were obtained with a Rigaku XRD diffractometer employing Cu Kα radiation (λ = 1.541838 Å). The X-ray was operated at 45 kV and 100 mA. Diffraction patterns were obtained using a scan rate of 0.5 deg/min with slits = 1mm. Powdered samples were mounted on glass slides by pressing the powder into an indentation on one side of the slide.

The mean crystallite size ($\bar{d}$) of the CeO_2 particles was determined from XRD line broadening measurements using the Scherrer equation [30]:

$$\bar{d} = k\lambda/\beta\cos\theta \qquad (1)$$

where λ is the X-ray wavelength, k is the particle shape factor, taken as 0.9 for cubic particles, and β is the full width at half maximum (fwhm), in radians, of the CeO_2 <111> line and θ is the diffraction angle. Semi-quantitative X-ray diffraction data were obtained by comparing CeO_2<111>/Al_2O_3<440> intensity ratios measured for catalyst samples with peak ratios measured for physical mixtures of CeO_2 and γ-Al_2O_3. A calibration

curve was made using a physical mixture of CeO_2 and γ-Al_2O_3 with different concentration (g_{CeO2}/g_{Al2O3}). This method assumes that cerium addition does not disrupt the γ-Al_2O_3 spinel and consequently does not affect the intensity of the Al_2O_3 <440> line. The error in this method was estimated to be approximately ± 20%.

XPS Analysis. XPS data were obtained using a Perkin-Elmer Surface Science instrument equipped with a magnesium anode (1253.6 eV) operated at 300W (15 kV, 20 mA) and a 10-360 hemispherical analyzer operated with a pass energy of 50 eV. Spectra were collected using a PC137 board interfaced to a Zeos 386SX computer. The instrument typically operates at pressures below 1 x 10^{-8} Torr in the analysis chamber. Samples were analyzed as powders dusted onto double-sided sticky tape. Binding energies for the catalyst samples were referenced to the Al_{2p} peak (74.5 eV). XPS binding energies were measured with a precision of ± 0.2 eV, or better.

Binding energies for the standard samples were referenced to the C_{1s} line (284.6 eV) of the carbon overlayer. Since charging was observed for the standard Ce^{3+} and Ce^{4+} samples studied, the C_{1s} charge reference may be less accurate that a Ce_{3d} derived charge correction. Thus, charge correction was done using the Ce_{3d} u''' peak (916.7 eV) from cerium oxide sample. Using the Ce_{3d} u''' reference energy, the binding energy of the C_{1s} peak measured for the CeO_2 standard was 284.6 eV. The Ce_{3d} u''' peak has been commonly used to compensate for sample charging in ceria photoreduction studies [31]. Pure CeO_2 (Aldrich) was used for the Ce^{4+} XPS spectrum and $CeAlO_3$ (just prepared) for Ce^{3+} XPS spectrum were used as standard compounds. $CeAlO_3$ was prepared by reduction of cerium oxide at 900°C under H_2 for 16 hours.

2.3 Results and Discussion

Precursor-Support Interaction. During this study, it was observed that Ce8N and Ce8NR catalysts show a similar behavior to the parameters varied during the preparation and thermal treatment. As a result, the data obtained from these samples will be treated and interpreted together. Figure 2.1 presents DRIFTS spectra of γ-Al_2O_3, CeO_2 and $Ce(OH)_4$. Characteristic for the alumina spectrum (a) is the presence of the 3690 cm^{-1} band, which is attributed to the free hydroxyl groups present on the surface. The broad band at around 3500 cm^{-1}, indicates that many of the hydroxyl groups are hydrogen bonded [32]. The other bands observed in the spectrum are due to the residual CO_2 and H_2O (1638 cm^{-1}) adsorbed on the alumina surface, hard to remove by simple nitrogen purging, and the bands around 1200-100 cm^{-1} are attributed to Al-O stretch and bend from alumina structure [32-34].

Due to the sensitivity of the DRIFTS analysis, several well defined bands for CeO_2 were observed which are otherwise hard to see using simple FTIR analysis. Figure 2.1. (b) shows the DRIFTS spectrum for neat CeO_2. As in the case of the alumina support (a), the free and coupled hydroxyl groups from the surface, can be easily distinguished. The bands observed at 1556 cm^{-1}, 1473 cm^{-1}, 1299 cm^{-1}, and 1034 cm^{-1} were attributed in a recent study made by Verduraz *et al.* [33], to the carbonate and carboxylate species present on the CeO_2 surface. The band at 1556 cm^{-1} corresponds to a carboxylate species, 1473 cm^{-1} and 1299 cm^{-1} to a bidentate carbonate and 1034 cm^{-1} to a monodentate carbonate surface species. The last type of carbonate species can be found

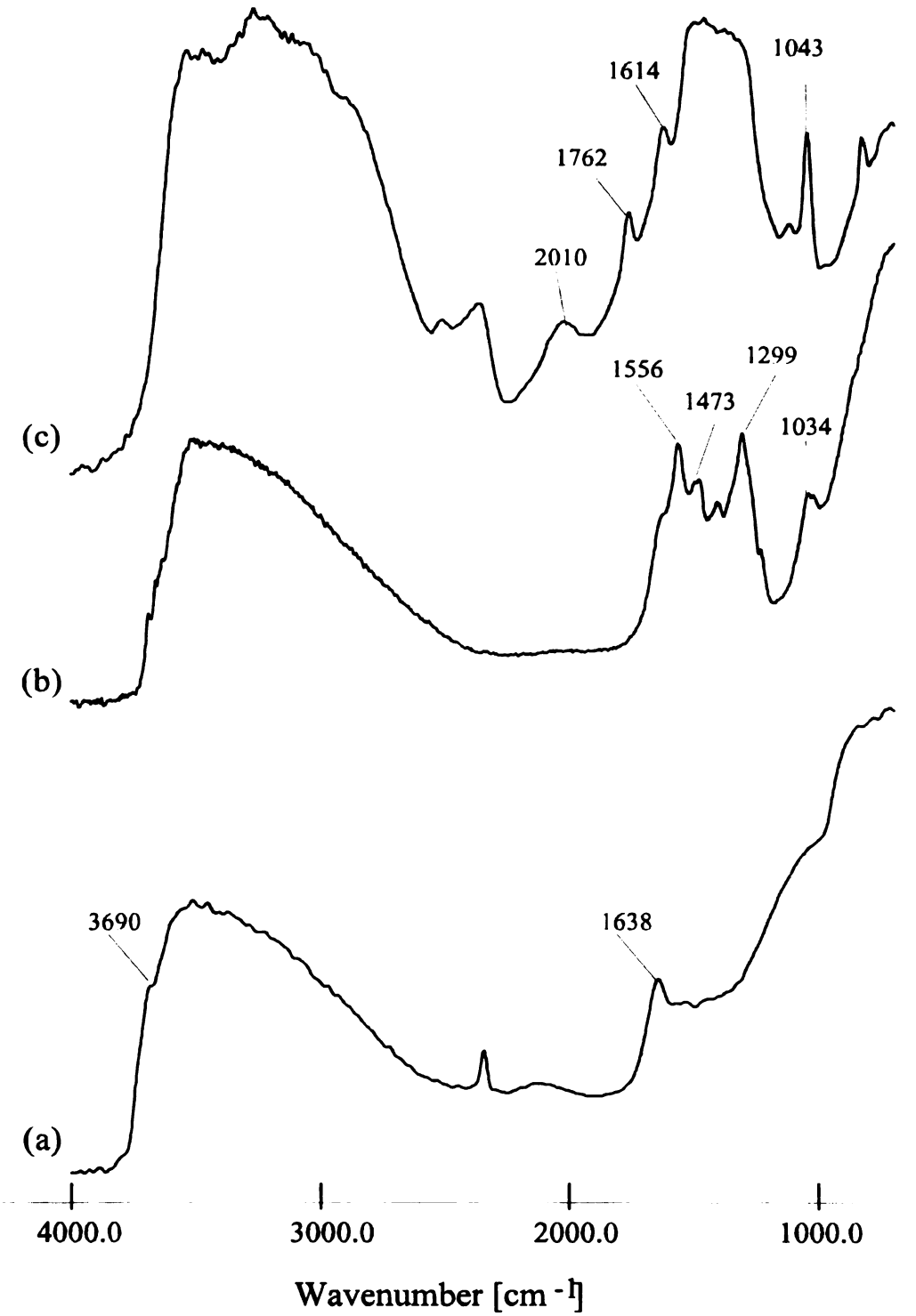

Figure 2.1 DRIFTS spectra of standard compounds: a) γ-Al_2O_3 support; b) CeO_2 obtained from pure cerium nitrate calcination; c) $Ce(OH)_4$

even after calcination at high temperature (800°C). The $Ce(OH)_4$ spectrum shown in Figure 2.1. (c), includes a broad band characteristic of the -OH stretch (3500-3000 cm^{-1}) involved in intramolecular hydrogen bonds, more intense bands characteristic of CO_2 and H_2O, bands characteristic of carboxyl or carbonyl surface species and bands characteristic of deformation of O-H bond (the broad band between 1500 - 1200 cm^{-1}) [34].

Figures 2.2 and 2.3 show the DRIFTS spectra of the Ce8N and Ce8NR catalysts, respectively, dried at 120°C (b) and calcined at 500°C (c) for comparison with the spectrum of pure γ-Al_2O_3 (a). In both cases, the spectra reveal the formation of $Ce(OH)_x$ species on γ-Al_2O_3 after drying the catalyst at 120°C. The process may be favored by the weak acidity of the alumina surface, which favors the formation of hydrated particles from Ce^{3+}/Ce^{4+}-nitrate solution. Simple water solvation and drying of cerium nitrate compounds led to identical DRIFTS spectra as the starting compounds. Together with the formation of the $Ce(OH)_4$ on the support, the alumina band at 3690 cm^{-1} corresponding to the free hydroxyl groups disappears and a strong increase in the intensity of the broad band around 3500-3000 cm^{-1} is observed, corresponding to hydrogen bonded hydroxyl groups. This fact suggests that the interaction between the cerium precursor and alumina support has only a physical nature, basically dipole-dipole interactions and hydrogen bonds. After calcination at 500°C [Figures 2.2 (c), and 2.3 (c)], the IR spectra of the catalysts became similar with the spectrum of the pure γ-Al_2O_3 support. The IR band at 3690 cm^{-1} corresponding to free surface hydroxyl groups from

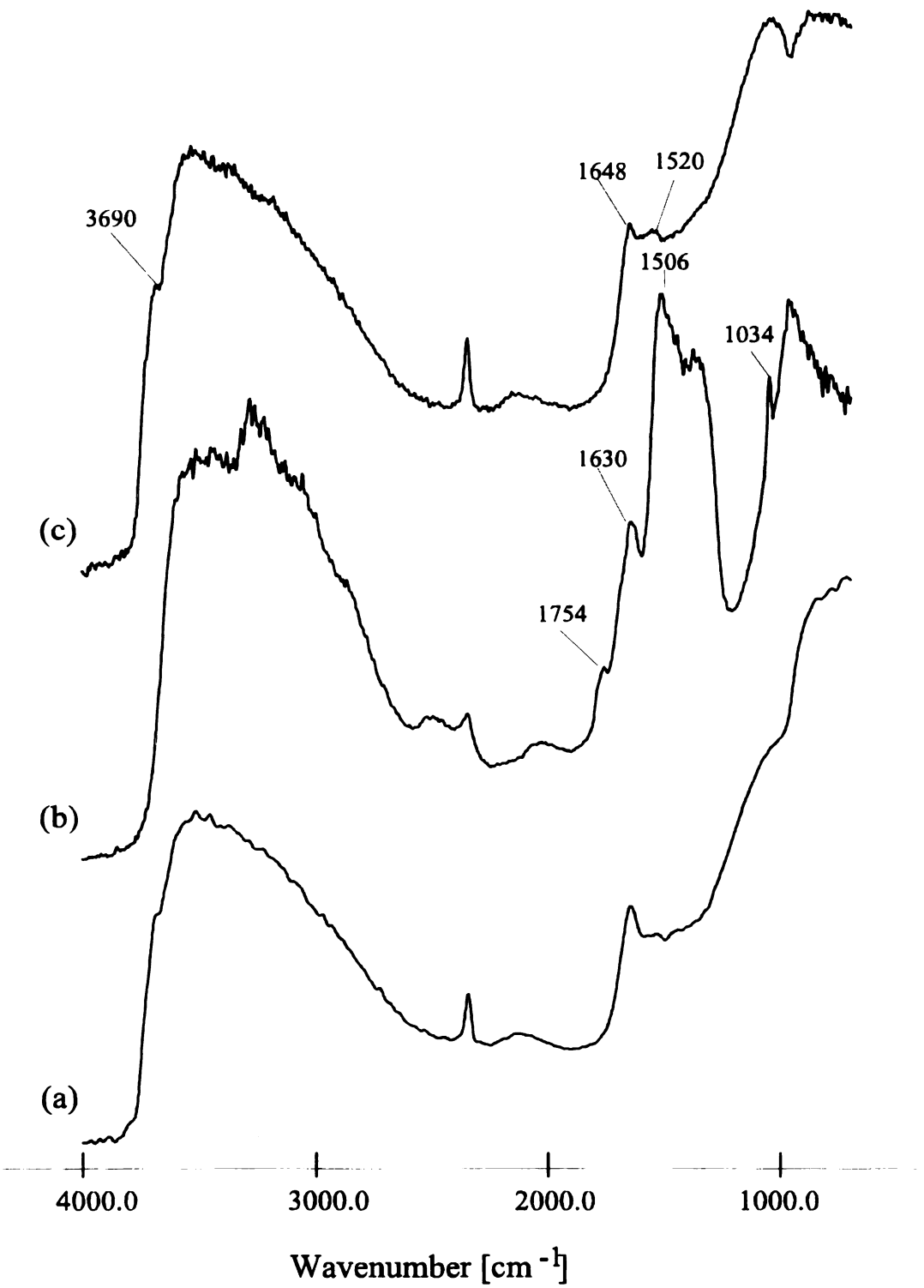

Figure 2.2 DRIFTS spectra acquired during preparation of the Ce8N catalysts: a) pure γ-Al_2O_3; b) dried at 120°C; c) calcined at 500°C

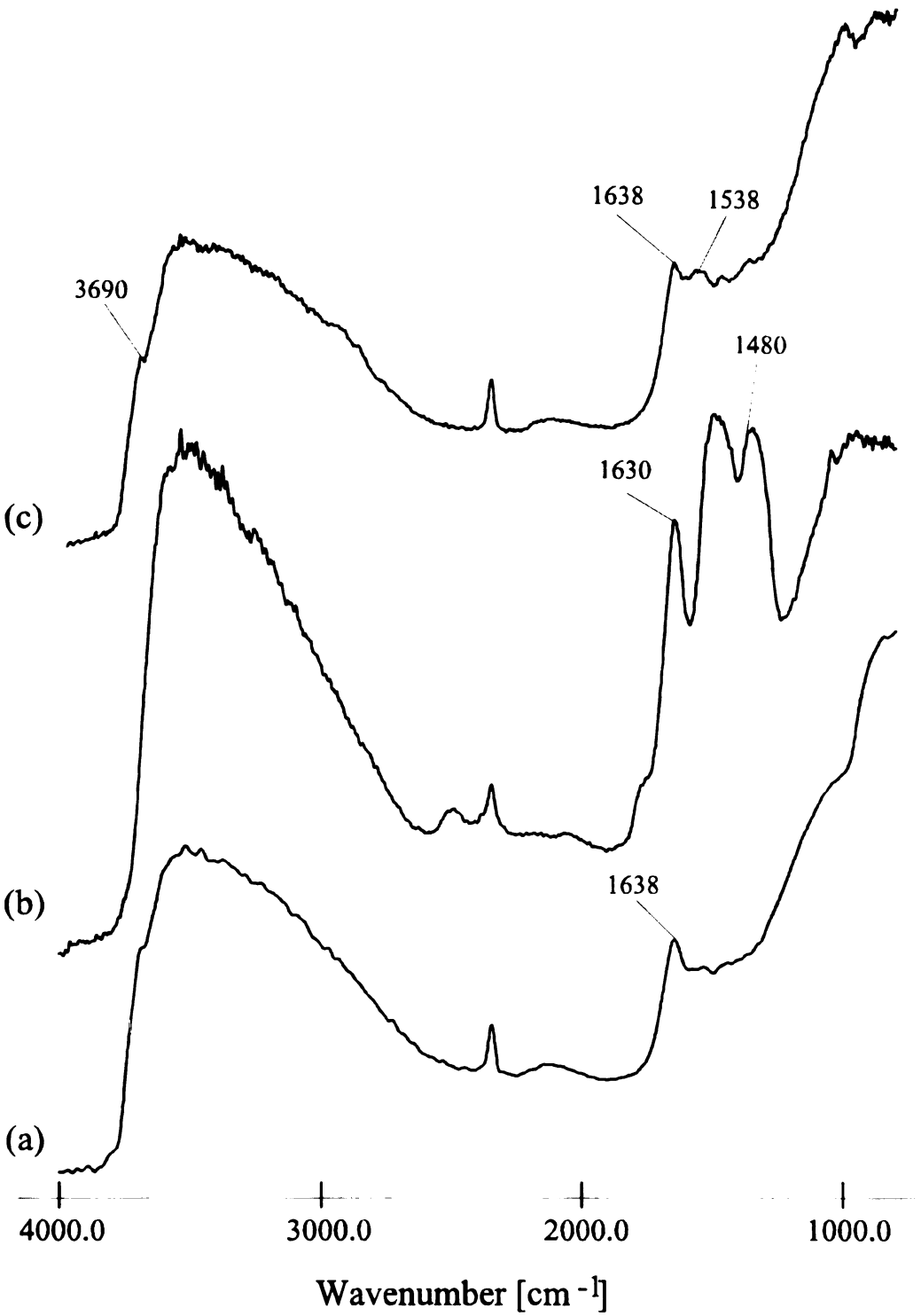

Figure 2.3 DRIFTS spectra acquired during preparation of the Ce8NR catalysts: a) pure γ-Al_2O_3; b) dried at 120°C; c) calcined at 500°C

alumina is regenerated in both cases, by removing the hydroxyl groups from the cerium species as CeO_2 is forming during calcination. Some remaining bands from bending -OH groups are still observable at 1520 cm^{-1} and 1100 cm^{-1}.

Figure 2.4, shows the DRIFTS spectra for the Ce8A catalysts acquired during impregnation and thermal treatment. As was mentioned before, the grafting process involves a chemical interaction between the support and precursor. The interaction of the cerium alkoxide with the support may take place either through a reaction with the hydroxyl groups involved in intramolecular hydrogen bonds or reaction with the free hydroxyl groups from the surface leading to the formation of Al-O-Ce-Alkoxide bonds [35]. If the Ce-OH phase is formed in the solution, the precursor-support interaction could be an intermolecular interaction through hydrogen bonds. During "simple grafting" DRIFTS spectra from Figure 2.4 (c) show the disappearance of the absorption band at 3690 cm^{-1} characteristic of the free hydroxyl groups from the γ-Al_2O_3 surface. The presence of the absorption bands at 2837 cm^{-1} characteristic of hydrocarbon C-H stretching, are observed for the pure cerium alkoxide precursor (not shown), and even for catalysts calcined at 200°C when all the solvent is removed from the catalyst supports. This observation supports the idea of a covalent bond interaction between the cerium alkoxide and alumina surface. In addition, no $Ce(OH)_4$ phase formation was observed during "simple grafting " as DRIFTS spectra of the dried catalyst indicates. After calcination, the DRIFTS spectra of the catalyst indicate the regeneration of the band corresponding to the free hydroxyl group from the support surface and the band at 1523

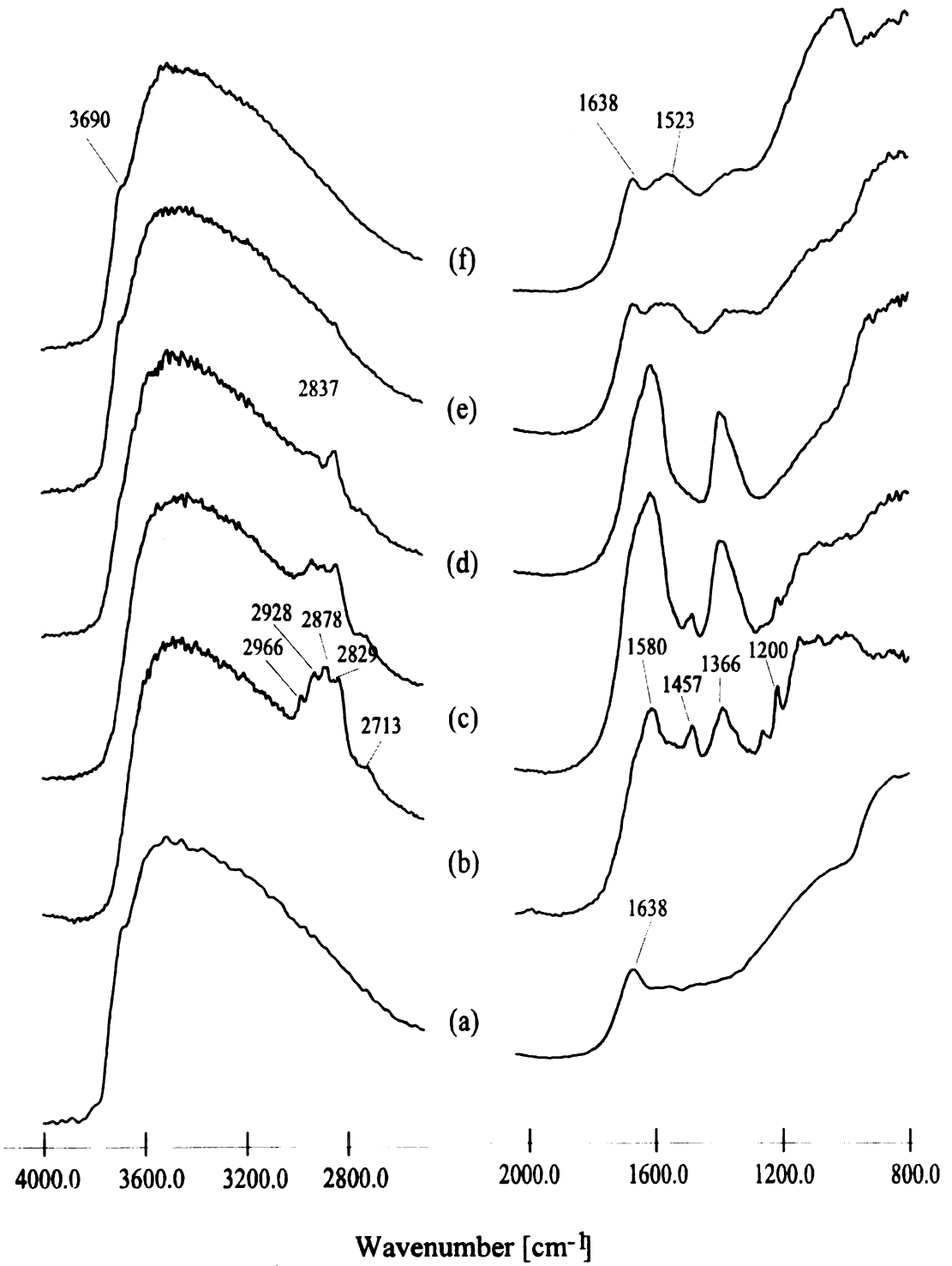

Figure 2.4 DRIFTS spectra acquired after thermal treatment of the Ce8A catalysts: a) pure γ-Al_2O_3; b) fresh; c) dried at 120°C; d) dried at 200°C; e) calcined at 300°C; f) calcined at 500° C

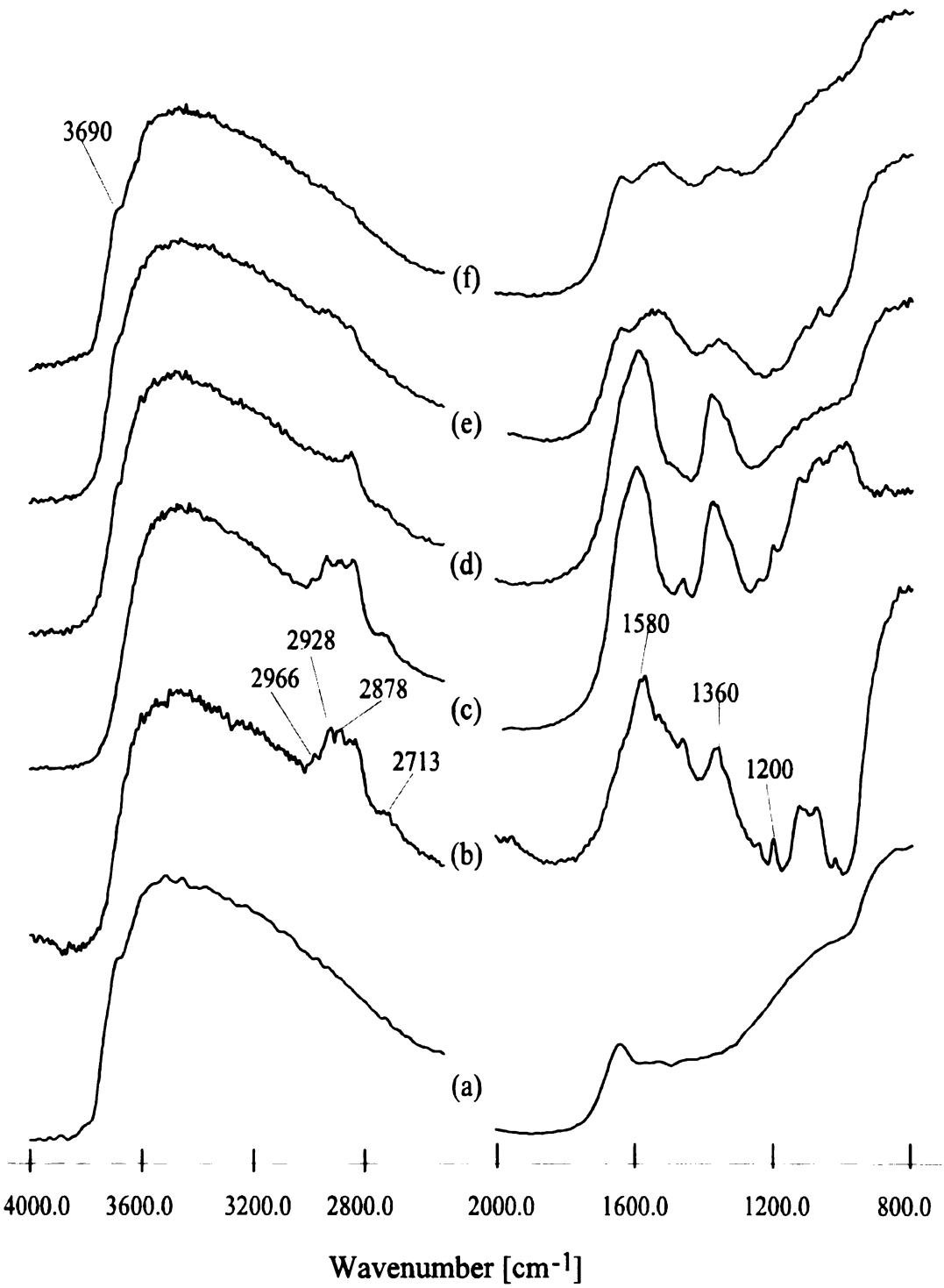

Figure 2.5 DRIFTS spectra acquired after thermal treatment of the Ce8HG catalysts: a) pure γ-Al_2O_3; b) fresh; c) dried at 120°C; d) dried at 200°C; e) calcined at 300°C; f) calcined at 500°C

cm^{-1} which can be assigned to a surface carboxylate species formed on CeO_2 [33].

Figure 2.5 shows DRIFTS spectra of the pure alumina support (a) for comparison with the spectra corresponding to the Ce8HG catalysts dried and calcined at different temperature (b-f). It can be observed from the spectrum (b) that the band corresponding to the free hydroxyl groups from the surface of pure alumina disappeared following impregnation with the cerium alkoxide solution. The solvent was removed from the catalyst by distillation under vacuum. Alkoxides exhibit characteristic C-O stretch bands in the 950-1200 cm^{-1} domain. Carboxylates presumably from oxidation of alkoxide exhibit a C-O stretching bands at 1580 cm^{-1}. Cerium-oxygen bands, which appear in the 500-250 cm^{-1} region, are hard to be observed due to the strong absoption bands of the support in this domain [36]. Figure 2.5 shows bands characteristic of the alkoxide even for catalysts calcined at 200° - 300°C (c-d), which may indicate that the cerium alkoxide species survived during impregnation and was dispersed on the support through a grafting reaction [see reaction (1)]. The intense band from 1580 cm^{-1} indicates also the formation of some metal (Al or Ce)-carboxylate species on the surface, during the "hot grafting" process. Comparison of the DRIFTS spectra of Ce8A in Figure 2.4 with those for Ce8HG in Figure 2.5 reveal similaries in absorption bands. This suggests that the grafting process occurs in the same way in both cases, but that the higher temperature and reflux conditions of the "hot grafting" may carry out the reaction more efficiently.

Bulk Characterization. Figure 2.6 presents XRD patterns for cerium species present on the alumina support during thermal treatment. Figure 2.6 a shows peaks that

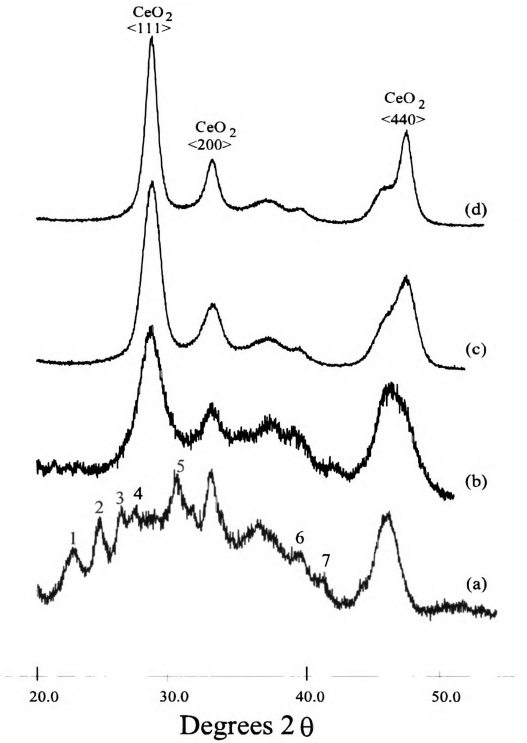

Figure 2.6 XRD patterns for Ce8N catalysts treated at different temperatures: a) 25°C; b) 120°C; c) 500°C; d) 800°C

correspond to the $Ce(NO_3)_6(NH_4)_2$ species (marked on the spectrum from 1 to 7). A DRIFTS spectrum of Ce8N catalyst dried at room temperature indicates bands similar with those observed for cerium ammonium nitrate (not shown). After drying above 125°C and removing the water from the system, the XRD patterns observed in Spectra 2.6 b-d, correspond mostly to the cerium oxide crystalline phase. DRIFTS spectra are consistent with this observation; the peaks observed by probing the catalysts surface correspond to the cerium hydroxide phase (see Figures 2.1 c, 2.2 b,c, and 2.3 b,c). As the temperature of the thermal treatment increases, the CeO_2 <111> peak becomes more intense and narrower. This fact is attributed to the growth of the CeO_2 crystalline phase with temperature. Figure 2.7 shows the XRD patterns of the Ce8A catalysts collected at different treatment temperatures. XRD patterns for Ce8A catalysts just dried at room temperature (25°C) after impregnation (a) and dried at 125°C in the oven, where only the XRD pattern corresponding to poorly crystalline CeO_2 species (very broad and less intense peaks) can be observed. Only after calcination at 500°C or higher can a broad XRD pattern for CeO_2 <111>, corresponding to the crystalline CeO_2 phase [Figure 2.7 (c-d)] be clearly observed. So, during impregnation and thermal treatment of the Ce8A catalyst, less or smaller crystalline CeO_2 particles are formed than in the case of Ce8N catalyst. In Figure 2.8 are presented the XRD patterns for γ-Al_2O_3 support (a) for comparison with the Ce8-catalysts prepared by using various precursors (b-e) after calcination at 500°C in air. Table 2.1 presents the CeO_2 particle size evaluated from the XRD pattern presented in Figure 2.8, using the Scherrer equation (1). The XRD peak at $2\theta = 28.5°$, corresponding to the main CeO_2 <111> peak, is utilized for our calculations.

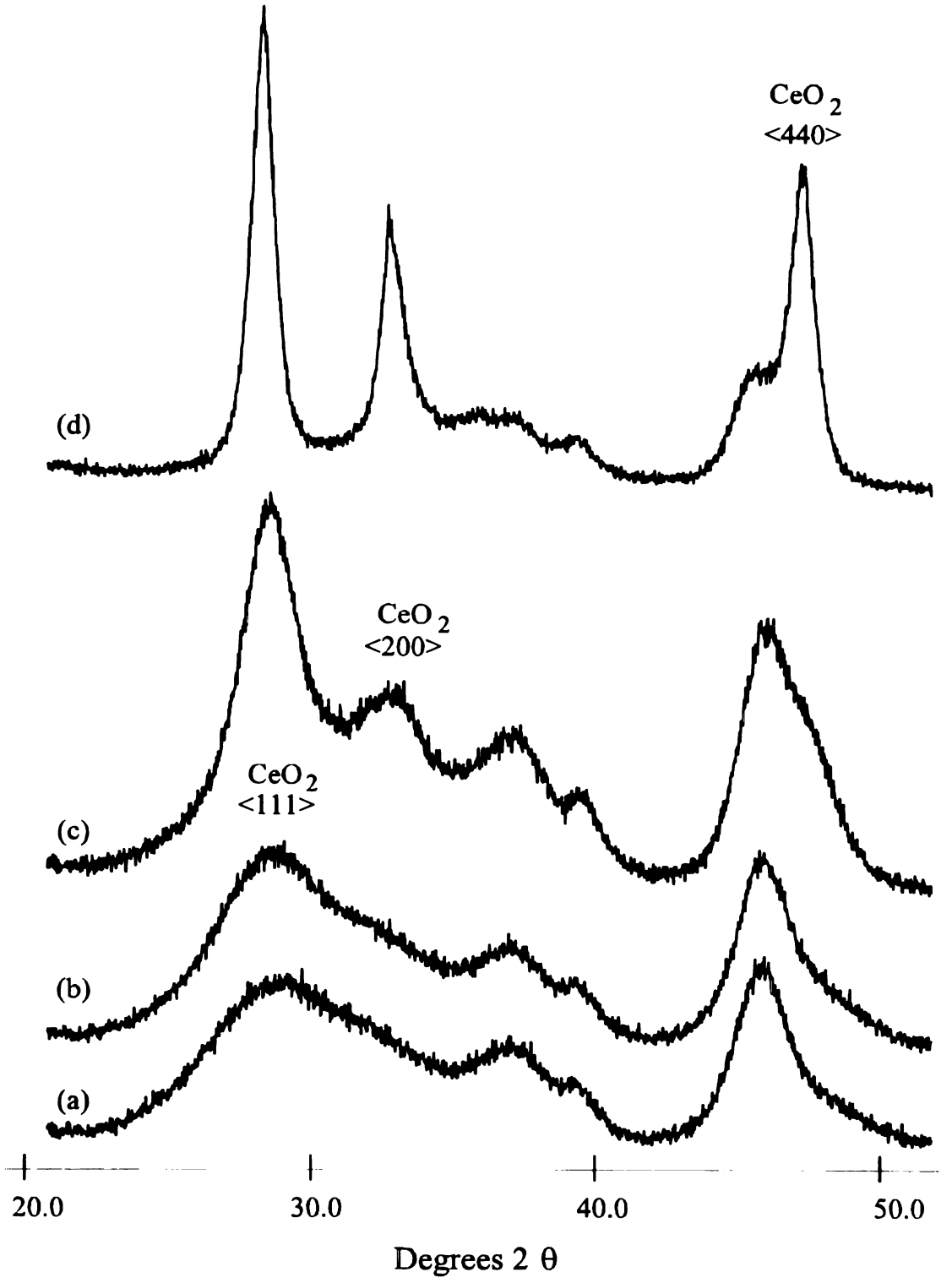

Figure 2.7 XRD patterns for Ce8A catalysts treated at different temperatures: a) 25°C; b) 120°C; c) 500°C; d) 800°C

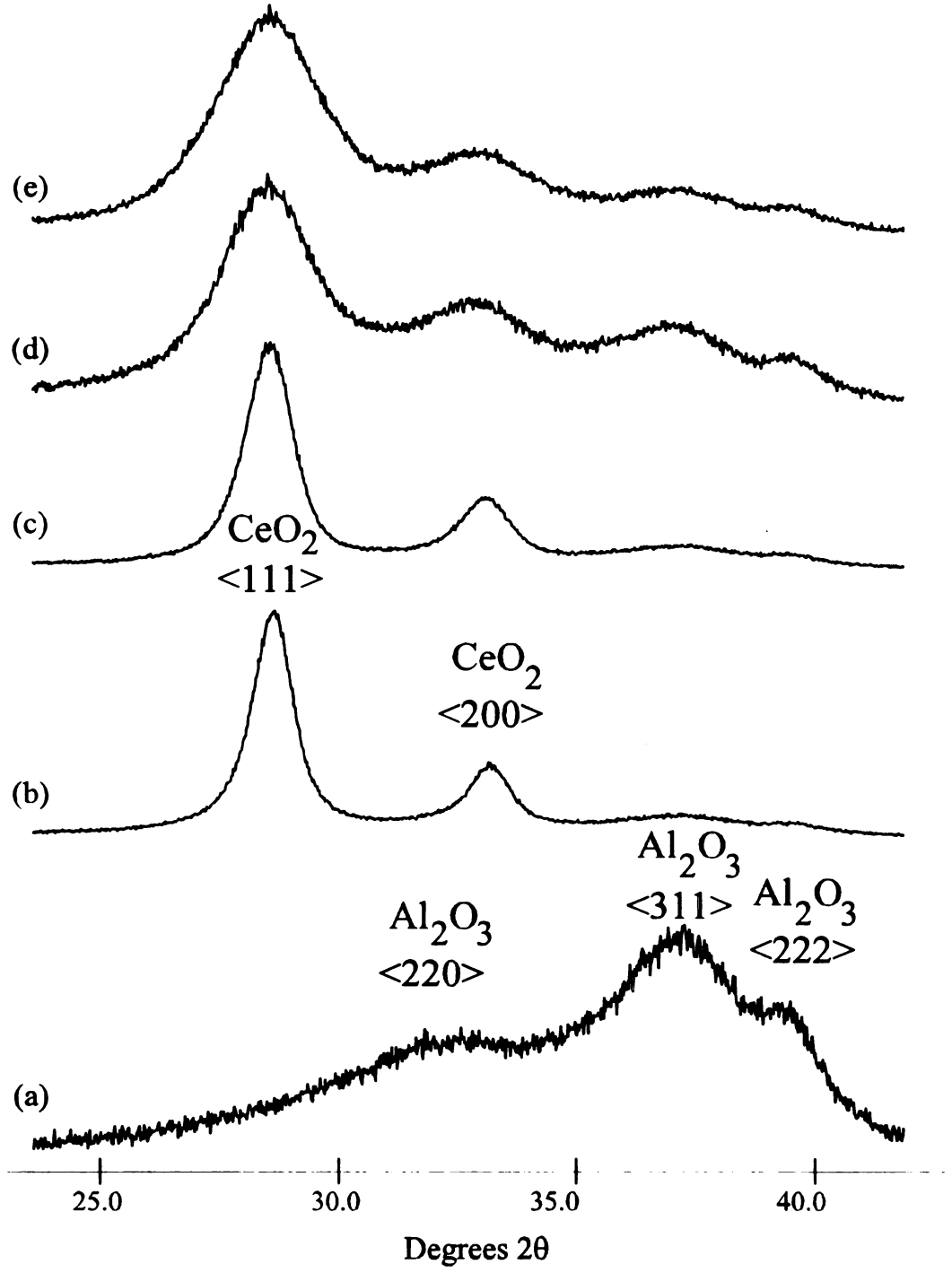

Figure 2.8 XRD patterns of the Ce8-series of catalysts calcined at 500°C: a) pure γ-Al_2O_3; b) Ce8N; c) Ce8NR; d) Ce8A; e) Ce8HG

Table 2.1 Semiquantitative XRD data and CeO_2 particle size determined from line broadening calculations for the Ce8-catalysts

	Ce8A	Ce8HG	Ce8NR	Ce8N
- after calcination at 500°C				
d [nm]	4.1	3.6	7.0	8.0
CeO_2 % crystalline	38	88	100	100
- after calcination at 800°C				
d [nm]	13.9	11.6	9.7	11.7
CeO_2 % crystalline	68	100	95	98.5

The particle size for Ce8N and Ce8NR catalysts are comparable (7-8 nm). The percentage of the CeO_2 crystalline phase present in the catalysts after calcination at 800°C, are 100% from the amount of cerium species added to the system during preparation, for both catalysts. This mean that almost all the cerium precursor used for impregnation was transformed in large crystallites. Among the four catalysts in Figure 2.8, the CeO_2 <111> peak is the lowest in intensity for Ce8A. The crystalline phase formed from the total amount of cerium used for impregnation reaches a value of only 38%. The rest of the cerium is present as amorphous CeO_x or very small CeO_2 crystallites (< 20Å). XRD analysis indicates that the Ce8HG catalyst calcined at 500°C has a much higher proportion of CeO_2 crystallites (88%) compared with the Ce8A catalyst obtained by the "simple grafting" technique (38%). On the other hand, the particle size for the Ce8A catalyst calculated from XRD line broadening (4.1 nm) is slightly larger than that for the Ce8HG catalyst (3.6 nm). The differences observed in CeO_2 particle size of the Ce8-catalysts can be attributed to the impregnation technique.

Based on previous data, transition metal alkoxide precursor led to a well dispersed oxide on the support following calcination at temperature above 500°C. In the case of cerium alkoxide, either "simple grafting" or "hot grafting" method led to the formation of CeO_2 crystallites larger than 3 nm, following calcination (far from a monolayer dispersion). This fact can be attributed to the polymerization of cerium alkoxide during the impregnation, which favor the formation of large CeO_2 particles, after calcination at 500°C and 800°C. The small difference in CeO_2 particle size observed between Ce8A and Ce8HG can be explained considering two opposite effects during catalyst preparation: i) the reflux and mixing conditions used in the case of "hot grafting" impregnation favored a better cerium dispersion; ii) the higher temperature during impregnation determined a higher percentage of CeO_2 crystalline phase for Ce8HG in comparison with Ce8A catalyst. However, the CeO_2 particle size is much lower than in the case of the Ce8N and Ce8NR catalysts, which corresponds to a better cerium dispersion. The small difference in CeO_2 particle size observed between Ce8A and Ce8HG can be explained by considering the reflux and mixing conditions used in the case of "hot grafting" impregnation which give the better dispersion. The higher temperature during impregnation apparently determines a greater crystalline percentage of CeO_2 phase for Ce8HG compared with Ce8A catalyst.

Figure 2.9 shows XRD patterns for the Ce8A and Ce8HG calcined at 500°C in comparison with those obtained after calcination at 800°C. For Ce8A catalysts (Figures 2.9 a and 2.9 b), calcination at higher temperature led to formation of larger CeO_2

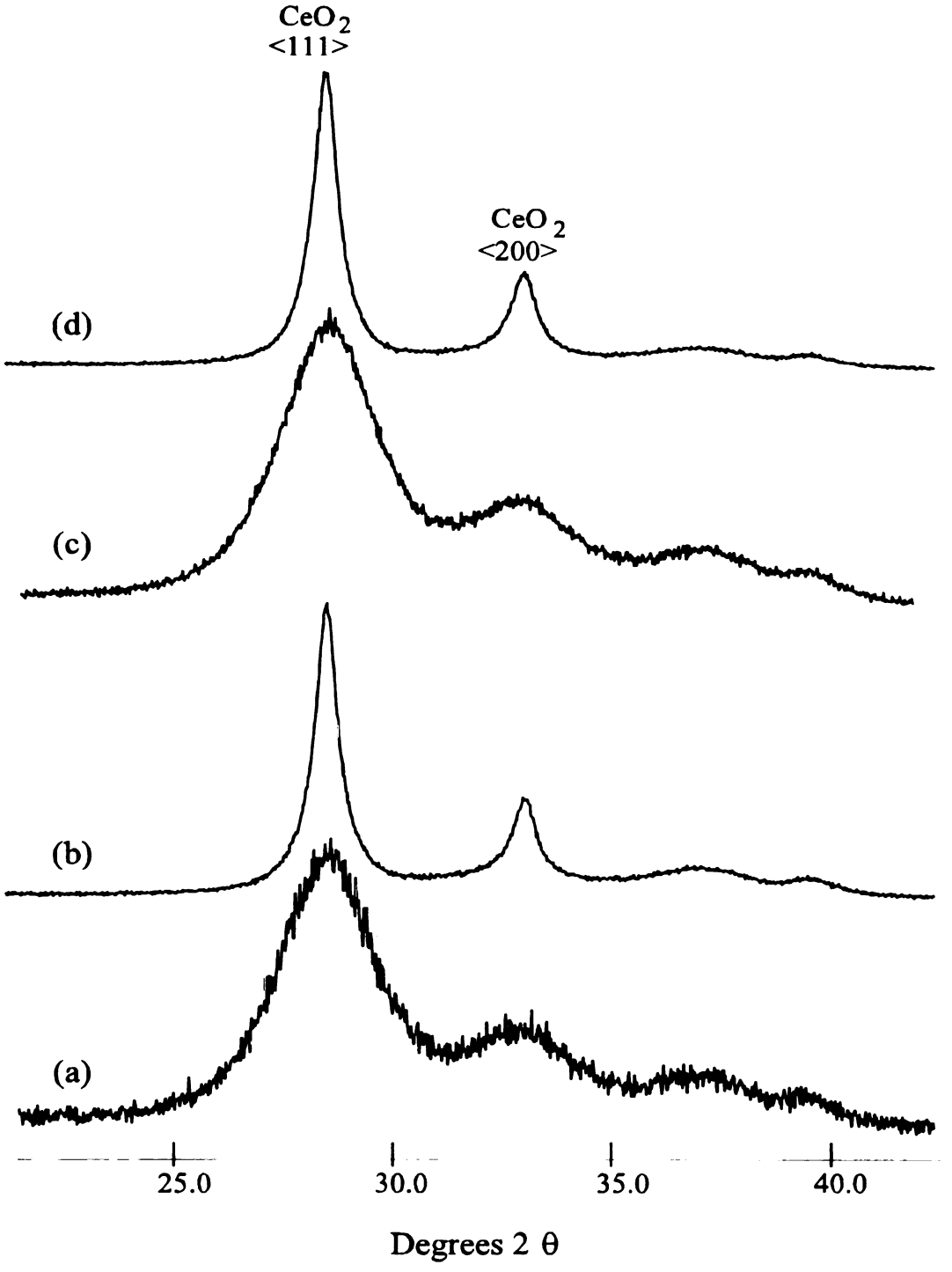

Figure 2.9 Comparison of XRD patterns of the Ce8HG and Ce8A catalysts calcined at different temperature: a) Ce8A calcined at 500°C; b) Ce8A calcined at 800°C; c) Ce8HG calcined at 500°C; d) Ce8HG calcined at 800°C

particles (13.9 nm) and a sharp increase in the crystalline CeO_2 phase (68%), as semiquantitative XRD analysis revealed. Figures 2.9 c and 2.9 d show the modification in the XRD pattern corresponding to CeO_2 <111> for the Ce8HG catalyst, calcined at 500°C and 800°C. Sample calcination at 800°C increases the particle size from 4.1 to 11.6 nm but does not significantly increase the crystallinity of the cerium phase (100%). This fact corresponds to a decrease in the cerium dispersion and suggests that the small crystallites are mobile enogh to get together and form large crystalline particles.

Cerium loading effect. Table 2.2 shows the variation in the BET surface areas of the Ce/Al_2O_3 catalysts as a function of Ce content. As can be observed, there are no real differences in the surface area of the catalysts following cerium impregnation. Since CeO_2 has essentially no porosity, a simple weight correction to the measurement values show that the surface area does not change significantly.

Table 2.2. The effect of cerium content on surface area and particle size evaluated from XRD line broadening of Ce*y*Al catalysts calcined at 500°C

Ce/Al Atomic	Ce*y*N		Ce*y*A		Ce*y*HG	
Ratio ($x10^2$)	S_a* [m^2/g]	d [nm]	S_a* [m^2/g]	d [nm]	S_a* [m^2/g]	d [nm]
0	200	-	200	-	200	-
1.0	194	4.1	188	a	191	a
2.0	195	4.9	175	2.8[b]	190	3.0
4.0	200	5.9	183	3.7	190	3.5
6.0	201	5.6	191	4.0	193	3.9
8.0	210	7.0	203	4.1	192	3.6

a - no CeO_2 XRD peaks detected; b - the value must be considered approximate due to the low intensity of the CeO_2 peak; * based on weight of alumina in the catalyst

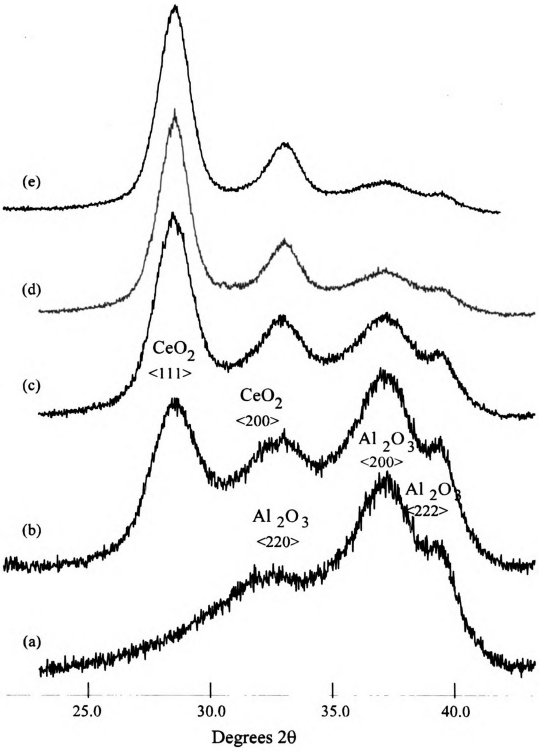

Figure 2.10 X-ray diffraction patterns measured for CeyN catalysts: a) Al_2O_3; b) Ce1N; c) Ce2N d) Ce4N; e) Ce6N

XRD analysis was used to examine the effect of cerium loading on the CeO_2 dispersion on γ-Al_2O_3 support when different impregnation techniques were used for catalyst preparation. XRD patterns for the Ce*y*N catalysts are shown in Figure 2.10, for Ce*y*A catalysts in Figure 2.11, and for Ce*y*HG in Figure 2.12. From these figures, the characteristic patterns corresponding to the CeO_2 crystalline phase can be observed clearly. The CeO_2 <111> peak has been used to evaluate the CeO_2 particle size using line broadening calculations. In each case, the relative intensities of the CeO_2 features and the particle sizes have increased with increasing Ce content. Table 2.2 shows the calculated values for CeO_2 particle size in the case of the Ce*y*N, Ce*y*A, and Ce*y*HG.

In the case of Ce*y*N catalysts (Figure 2.10), CeO_2 particle sizes increased with increasing cerium loading from 4.1 nm in the case of the Ce1N catalysts to 7.0 nm for the Ce8N catalyst. The diffraction pattern of the Ce1A catalyst (Figure 2.11) showed only lines characteristic for the γ-Al_2O_3 carrier. For Ce*y*A catalysts with Ce/Al atomic ratios $\geq$ 0.02, peaks characteristic of CeO_2 are observed. The relative intensities of the CeO_2 lines increase with Ce loading. The CeO_2 particle size calculated for the Ce*y*A catalysts with $y \leq 4.0$ are very close to each other (3.7 nm compared with 4.1 nm), but significantly smaller than the values obtained for Ce*y*N catalysts of the same composition. A similar trend is observed for the Ce*y*HG catalysts as is seen in Figure 2.12. For the Ce1HG catalyst, no pattern specific to CeO_2 crystalline phase is observed, but as the cerium loading is increased, $y \geq 2.0$, the line characteristic of CeO_2 <111> is well defined. The relatively small particle size for Ce*y*HG catalysts may indicate a better dispersion of the CeO_2 crystalline phase or amorphous phase formation.

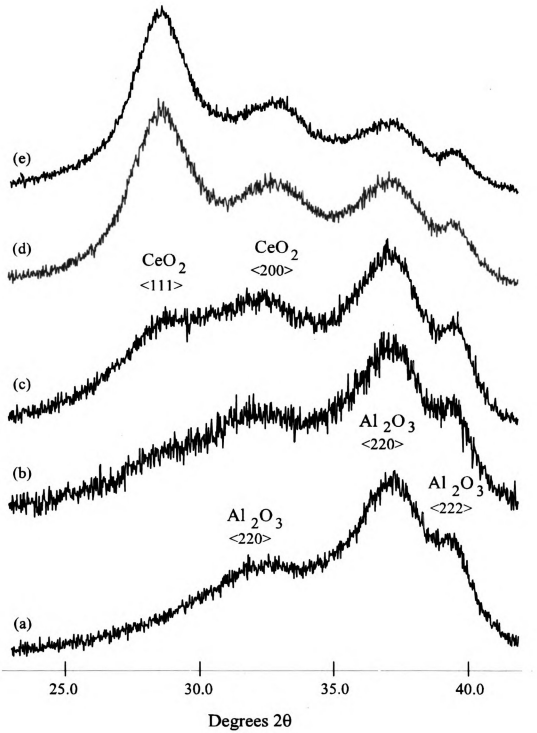

Figure 2.11 X-ray diffraction patterns measured for Ce*y*A: a) Al_2O_3; b) Ce1A; c) Ce2A; d) Ce4A; e) Ce6A

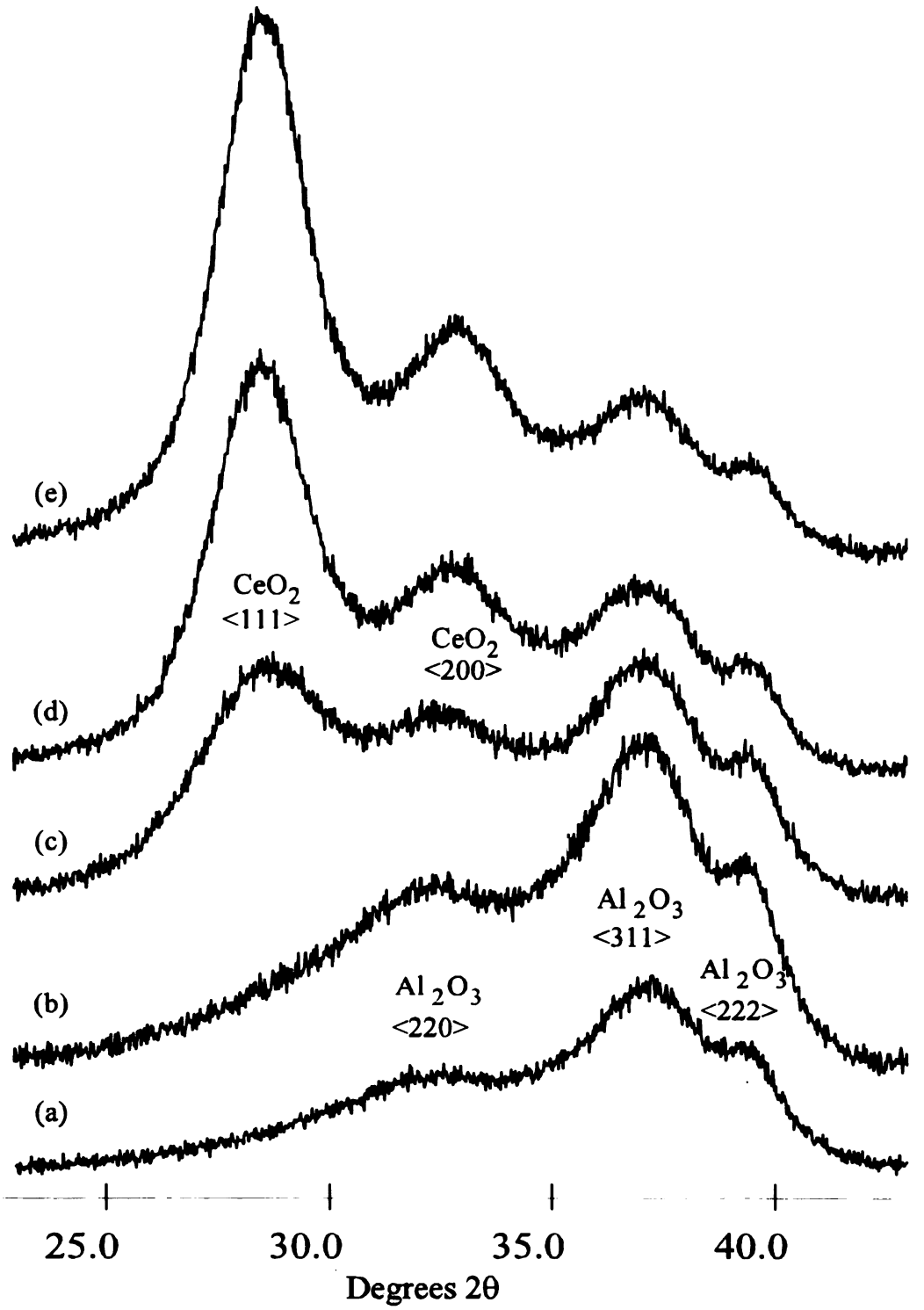

Figure 2.12 X-ray diffraction patterns measured for Ce*y*HG catalysts: a) Al_2O_3; b) Ce1HG; c) Ce2HG;d) Ce4HG; e) Ce6HG

Table 2.3 Concentration of crystalline CeO_2 in Ce*y*N, Ce*y*A and Ce*y*HG catalysts calculated from quantitative XRD[a] data

Ce/Al Atomic Ratio CeO_2 ($x10^{-2}$)	Weight % CeO_2 in Catalysts	Weight % CeO_2 crystalline from the total cerium added		
		Ce*y*N	Ce*y*A	Ce*y*HG
1.0	3.4	74	b	b
2.0	6.8	93	3	43
4.0	13.5	100	38	64
6.0	20.3	100	42	67
8.0	26.9	100	38	88

a - valid for CeO_2 particle size > 3.0 nm.
b - no CeO_2 XRD peaks detected for this catalyst.

Table 2.3 shows the concentration of crystalline CeO_2 phase in the Ce*y*N , Ce*y*A and Ce*y*HG catalysts determined from semiquantitative XRD analysis. In all cases, the amount of crystalline CeO_2 increases with increasing Ce loading.

For Ce*y*N catalyst, the amount of CeO_2 crystalline phase is close to the weight percent of CeO_2 used for catalyst preparation (Table 2.3). This implies that all the cerium nitrate used for the catalyst impregnation was transformed into crystalline cerium oxide phase. The formation of crystalline CeO_2 phase was attributed to the dehydration of the $Ce(OH)_4$ species formed on the alumina surface after impregnation with the aqueous nitrate solution [27, 37]. These led after calcination at 500°C to large CeO_2 crystallites due to dehydration of the $Ce(OH)_4$ formed after impregnation and drying. The differences between the experimental and initial values for cerium oxide concentration present in the catalysts (13.5% versus 14.7% in the case of the Ce4N catalyst) are in the range of the 20% error considered acceptable for the semiquantitative XRD calculations. The amount of crystalline CeO_2 present in the Ce*y*A series (Table 2.3) increases with

increasing Ce content; however, the concentrations are significantly lower than the amount of cerium oxide present in the catalysts. This fact can be attributed to the formation of cerium amorphous phase or small crystallites (< 2 nm). Table 2.2 shows the variation in the CeO_2 particle size as a function of Ce content for the Ce*y*A catalysts determined from XRD line broadening calculations.

A similar analysis of the Ce*y*HG catalysts shows that the amounts of CeO_2 crystalline phase in these catalysts are lower than the amounts of cerium used for catalyst preparation but higher than for the CeyA series. As in the case of the Ce*y*A catalysts, this finding can be attributed either to an amorphous phase or to small CeO_2 crystallites. If small CeO_2 crystallites are formed on the alumina support, it would suggest that a well dispersed cerium phase is formed on the alumina surface. However, previous data presented in the first part of this work has indicated that cerium alkoxide solution agglomerates on the alumina surface during impregnation due to polymerization of the alkoxide, which competes with the grafting reaction. As data for Ce*y*A and Ce*y*HG series have shown, grafting impregnation led to formation of more amorphous cerium oxide The size of crystalline CeO_2 range from 3.0 to 3.9 nm, close to the detection limit of the XRD analysis. Incepient wetness impregnation using cerium nitrate (Ce*y*N series) led to the formation of large CeO_2 particles with a high degree of crystallinity.

As a conclusion, the chemical instability, low concentration of the cerium alkoxide precursor used for impregnation, and the incomplete grafting reaction of the alkoxide with the support which favored cerium alkoxide polymerization led after calcination at 500C mostly to amorphous phase and large CeO_2.

Cerium Oxidation State. Figure 2.13 show the Ce XPS spectra of the standard $Ce^{3+}AlO_3$ (a) and $Ce^{4+}O_2$ (b) compounds. The XPS Ce_{3d} spectra of standard compounds are complicated due to hybridization of the Ce 4f with ligand orbitals and fractional occupancy of the valence 4f orbital [38-40]. The Ce_{3d} spectrum obtained for $CeAlO_3$ [Figure 2.13 (a)] is relatively a simple one, containing two major $3d_{5/2}$ peaks at 883.1 eV (v) and 886.5 eV (v') and the main $Ce3d_{3/2}$ features which appear at 900.1 eV (u) and 905.5 eV (u'). These peaks have been assigned to cerium with mixed $4f^1$ and $4f^2$ orbital configurations. The Ce3d spectrum measured for CeO_2 [Figure 2.13. (b)] contains three main $3d_{5/2}$ features at 883.2 eV (v), 889.2 eV (v"), and 899.4 eV (v"'). The three main $Ce3d_{3/2}$ features appear at 901.1 eV (u), 907.7 eV (u"), and 917.3 eV (u"'). The high binding energy doublet v"'(u"') has been assigned to cerium with $4f^0$ orbital configuration. The v" and v (u" and u) doublets are assigned to cerium with mixed $4f^1$ and $4f^2$ orbital configurations. These states appear due to the core hole potential in the final state and the 4f hybridization in the initial state [39-44]. As can be observed, cerium compounds which contain only Ce^{3+} do not have u"'(v"') peaks characteristic of the $4f^0$ orbital configuration. This observation implies that the u"' peak can be used to indicate the presence of Ce^{4+} on the catalysts. However, the relative intensity of the u"' feature cannot be used to determine the amount of Ce^{4+} present in the catalysts unless the dispersions of the Ce^{4+} and Ce^{3+}-phases are known and it is assured that cerium photoreduction does not occur [41, 42].

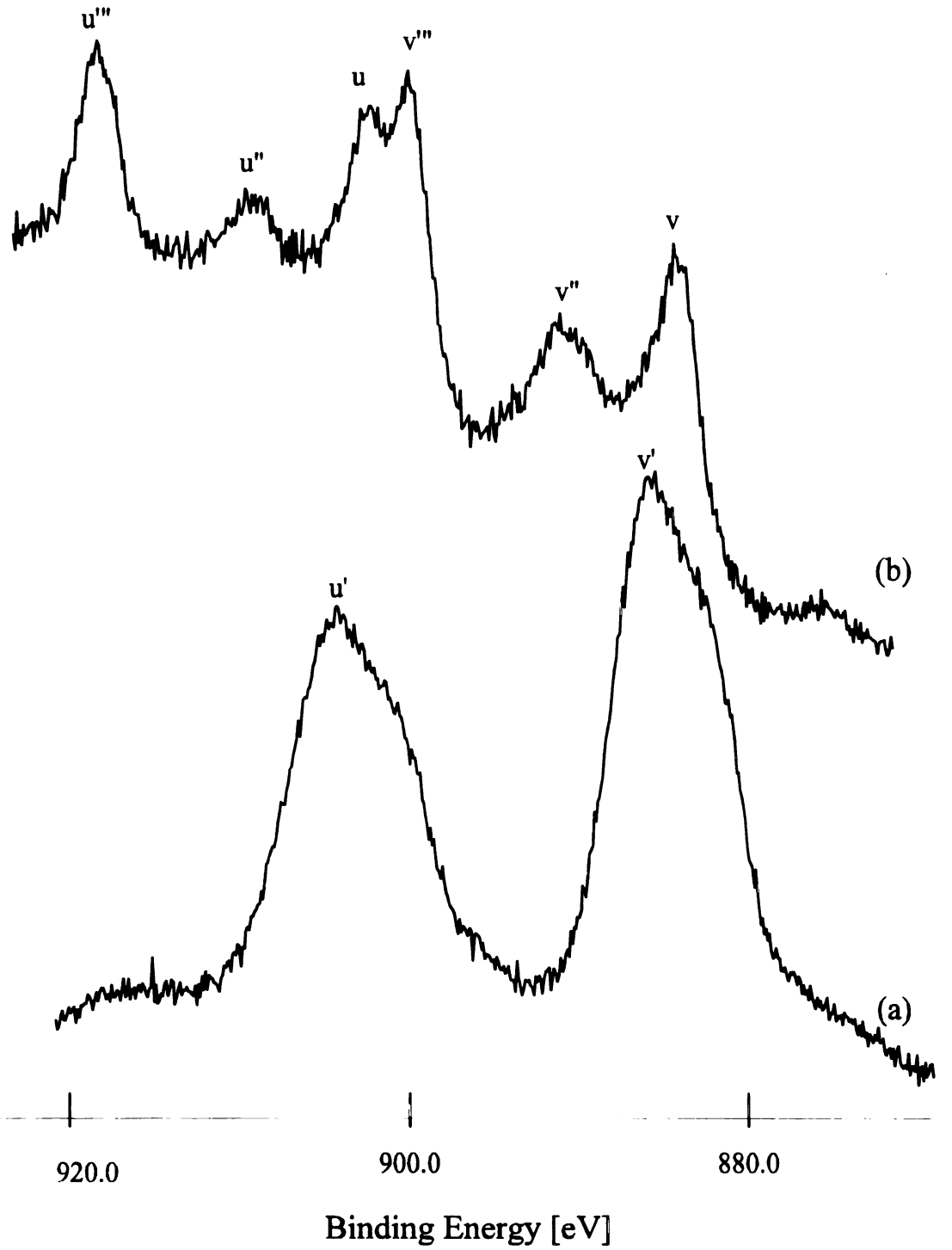

Figure 2.13 Ce XPS spectra for standard cerium compounds: a) $Ce^{3+}AlO_3$; b) $Ce^{4+}O_2$

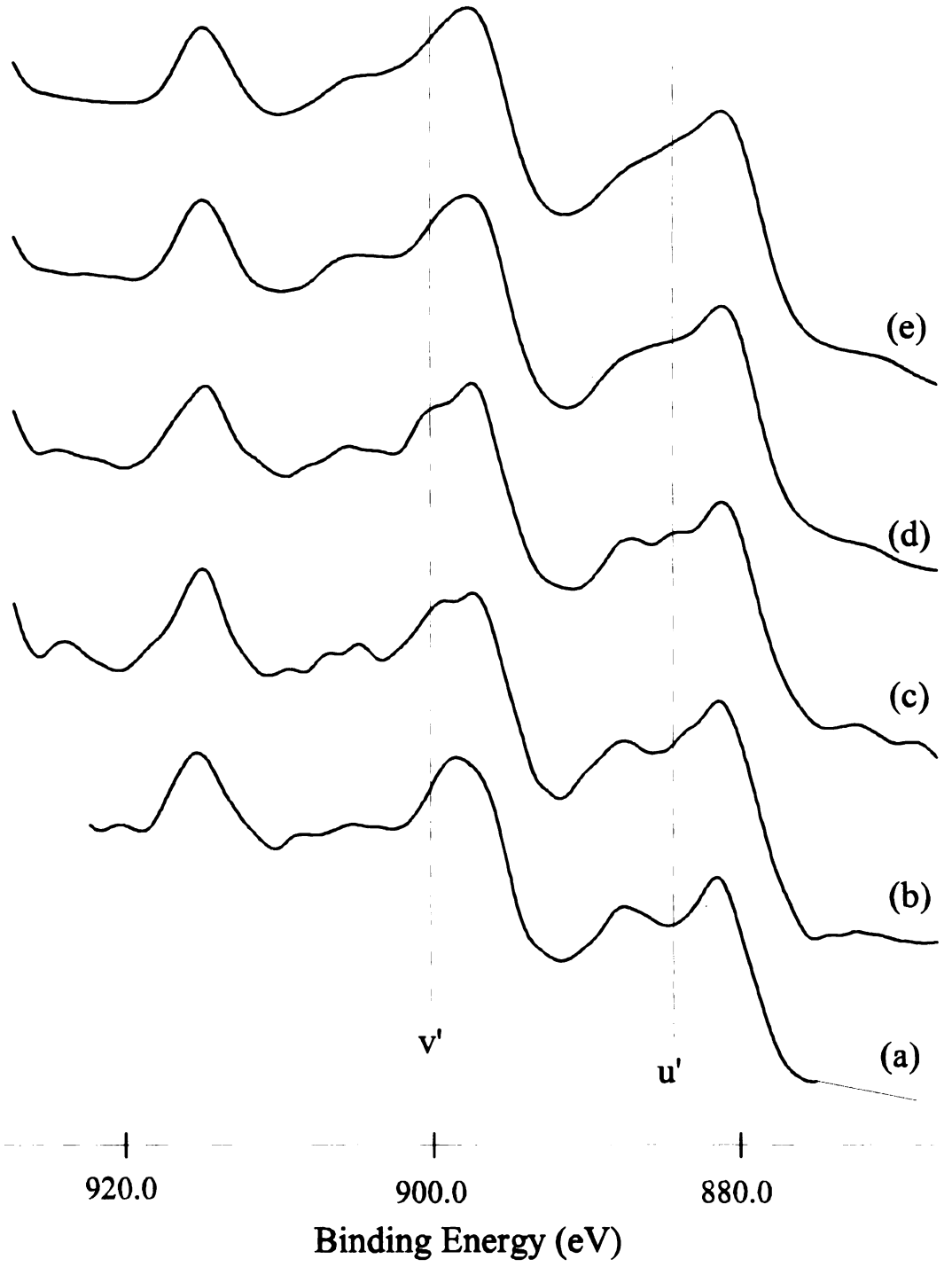

Figure 2.14 Ce XPS photoreduction spectra for Ce8A catalyst, calcined at 800°C after: a) 5 min.; b) 15 min.; c) 30 min.; d) 1 h; e) 4 h, of scanning

Figure 2.14 shows the Ce XPS spectra for Ce8A catalyst, calcined at 800°C, collected at different X-ray exposure times. For short scanning time (Figure 2.14 a) the surface cerium phase is present as Ce^{4+}. As the scanning time increases [Figure 2.14 (b-e)], the v'-peak intensity increases corresponding to the appearance of surface Ce^{3+} species. Previous studies have indicated that CeO_2 undergoes photoreduction during XPS analysis in high vacuum due to intense heating of the sample surface, the presence of free electrons into the chamber and the crystallinity of the exposed particle [43-46]. Park and Ledford [47] have shown that the photoreduction of cerium is also a function of CeO_2 crystallinity. The amorphous phase is reduced more than the crystalline one. The results in Figure 2.14 indicate that cerium supported on γ-Al_2O_3 is photoreduced even in the case of the catalyst calcined at 800°C. The photoreduction and the relatively low cerium dispersion found for the catalyst in this study preclude XPS quantitative analysis of Ce^{3+}/Ce^{4+} supported species. For Ce8N, Ce8NR and Ce8HG catalysts, XPS spectra indicate the presence of cerium as Ce^{4+} species, being present mostly as CeO_2 crystalline phase. In this case, X-ray photoreduction during XPS analysis is significantly decreased due to the higher crystallinity of the cerium species.

2.4. Conclusions

On the basis of the results obtained from bulk and surface techniques used to characterize the various cerium modified γ-Al_2O_3 catalysts obtained by using different precursors, we can conclude that: 1) $Ce^{3+/4+}$-nitrate precursors, impregnated via the incipient wetness method, led to large CeO_2 crystallites; 2) the grafting technique, using a cerium alkoxide precursor, is an alternative preparation method for γ-Al_2O_3 impregnation;

the grafting process takes place through a reaction between surface hydroxyl groups (free or hydrogen bonded) from the support and cerium precursor; during this process no evidence of $Ce(OH)_4$ formation is observed; 3) Simple grafting led to only a slight improvement in cerium dispersion compared with the traditional incipient wetness approach using cerium nitrate; specific to the grafting method is the formation of Ce^{4+}-amorphous phase on the support surface after calcination at 500°C; 4) XRD data show variations in crystallinity and cerium dispersion on alumina surface, when different precursors and Ce-loadings were used for catalyst preparation; 5) XPS data indicates that cerium is present on the catalyst surface as Ce^{4+} unless it is photoreduced during analysis.

2.5 References

1. Ledford, J. S.; Houalla, M.; Proctor, A.; Hercules, D. M. *J. Phys. Chem.* **1989**, *93*, 6770-6777.
2. Barrault, J.; Guilleminot, A.; Achard, J. C.; Paul-Boncour, V.; Percheron-Guegan, A.; *Appl. Catal.* **1986**, *21*, 307-312.
3. Fleisch, T. H.; Hicks, R. F.; Bell, A. T. *J. Catal.* **1984,** *87*, 398-413.
4. Reick, J. S.; Bell, A. T. *J. Catal.* **1985**, *96*, 88-105
5. Diwel, A. F.; Rajaram, R. R.; Truex, T. J. *Catalysis and Automotive Pollution Control II* Edit by Crucq, A. **1991**, Elsevier, Amsterdam, 139-152.
6. Pembo, J. M.; Lenzi, M.; Lenzi, J.; Lebugle, A. *Surf. Inter. Anal.* **1990**, *15(11)*, 663-668.
7. Yu-Yao, Y.F.; Kummer, J.T. *J. Catal.* **1987**, *106*, 307-312.
8. Chojnacki, T.; Krause, K.; Schmidt, L.D. *J. Catal.* **1991**, *128(1)*, 161-165.
9. Schaper, H.; Doesburg, E. B. M.; VanReijen, L. L. *Appl. Catal.* **1983**, *7*, 211-220.
10. Oudet, F.; Courtine, P.; Vejux, A. J. *J. Catal.* **1988**, *114*, 112-118.
11. Yao, H. C.; Yu-Yao, Y. F. *J. Catal.* **1984**, *86*, 254-265.
12. Yang, J. K.; Swartz, W. E. *Spectrosc. Lett.* **1984**, *17(6&7)*, 331-337.
13. Gaugin, R.; Graulier, M.; Papee, D. *Adv. Chem. Ser.* **1975**, *143*, 147-149.
14. Koberstein, E. *Unst. St. Proc. Catal.*, Matros, Y.S., Ed., **1990**, 643-648.
15. Yamaguchi, T.; Ikeda, N.; Hattony, H.; Tanabe, K. *J. Catal.* **1981**, *67*, 324-330.
16. Raen, S.; Braten, N. A.; Grepstad, J. K.; Qui, S. L. *Phys. Scr.* **1990**, *41(6)*, 1001-1002.
17. Nunan, J.; G.; Robota, H. J.; Cohn, M. J.; Bradley, S. A. in *Catalysis and*

Automotive Pollution Control II, ed Crucq, A. Elsevier, Amstredam, **1991**, 21-230.

18. Rodriguez, R. I.; Guerrero, R. A.; Fierro, J. L. G. *Appl. Surf. Sci.* **1989**, *40(3)*, 239-241.
19. Silver, R. G.; Summers, J. C.; Williamson, W. B. in *Catalysis and Automotive Pollution Control II*, ed. Crucq, A. Elsevier, Amsterdam, **1991**, 167-180.
20. LeNormand, F.; Hilaire, L.; Kili, K.; Krill, G.; Maire, G. *J. Phys. Chem.* **1988**, *92*, 2561-2568.
21. Shyu, J. Z.; Otto, K.; Watkins, W. L. H.; Graham, G. W.; Belitz, R. K.; Gandhi, H. S. *J. Catal.*, **1988**, *114*, 23-33.
22. Miki, T.; Ogawa, T.; Ueno, A.; Matsuura, S.; Sato, M. *Chem. Lett.* **1988**, 565-568.
23. Haneda, M.; Mizushima, T.; Kakuta, N.; Ueno, A.; Sato, Y.; Matsuura, S.; Kasahara, K.; Sato, M. *Bull. Chem. Soc. Jpn.* **1993**, *66*, 1279-1288.
24. Mizukami, F.; Maeda, K.; Watanabe, M.; Masuda, K.; Sano, T.; Kuno, K. in *Catalysis and Automotive Pollution Control II,* Edit by Crucq, A. **1991**, Elsevier, Amsterdam, 557-568.
25. Leclercq, G.; Danthy, C.; Mabilon, G.; Leclercq, L. in *Catalysis and Automotive Pollution Control II*, Edit by Crucq, A. **1991**, Elsevier, Amsterdam, 181-194.
26. Weibel, M.; Garin, F.; Bernhardt, P.; Maire, G.; Prigent, M. in *Catalysis and Automotive Pollution Control II*, Edit by Crucq, A. **1991**, Elsevier, Amsterdam, 95-205.
27. Munuera, G.; Fernandez, A.; Gonzalez-Elipe, A. R. in *Catalysis and Automotive Pollution Control II*, Edit by Crucq, A. **1991**, Elsevier, Amsterdam, 207-219.
28. *Powder Diffraction File*, Inorganic Phases, JCPDS, **1983**.
29. Bell, A. T. in *Vibrational Spectroscopy of Molecules on Surfaces* Ed. Yates, J. T. **1987,** New York, 105-134.
30. Klug, H.P.; Alexander, L.E. in *X-ray Diffraction Procedures for Polycrystalline and Amorphous Materials,* 1-st Ed. Wiley, New York, **1954**.
31. Paparazzo, E.; Ingo, G. M.; Zacchetti, N. *J. Vac. Sci. Technol. A*, **1991**, *9*, 1416.
32. Peri, J. B. *J. Phys. Chem.* **1965**, *69(1)*, 211-219.
33. Verduraz, F. B.; Bensalem, A. *J. Chem. Soc. Faraday Trans.* **1994**, *90(4),* 653-657.
34. Nakamoto, K. in *Infrared and Raman Spectra of Inorganic and Coordination Compounds*, 4-th Ed. Wiley, New York, **1986**, 231, 384.
35. Kifenski, J.; Baiker, A.; Glinski, M.; Dollenmeier, P.; Wokaun, A. *J. Catal.* **1986**, *101*, 1-11.
36. Fujimori, A. *Phys. Rev. B*, **1983**, *28(4),* 2281-2283.
37. Dulamita, N.; Pop, A.; Corbeanu, V. *Studia*, **1984**, *29*, 3-11.
38. Wuilloud, E.; Delley, B.; Schneider, W. D.; Baer, Y. *Phys. Rev. Lett.* **1984**, 202-207.
39. Fujimori, A. *Phys. Rev. Lett.* **1984**, *53*, 2518.
40. Wuilloud, E.; Delley, B.; Schnieder, W. D.; Baer, Y. *Phys. Rev. Lett.* **1984**, *53*, 2519.
41. Jo, J.; Kotani, A. *Phys. Scrp.* **1987**, *35*, 570-575.
42. Praline, G.; Koel, B. E.; Hance, R. L.; Lee, H. I.; White, J. M. *J. Electron Spec.*

Relat. Phenom. **1980**, *21*, 17-46.
43. El Fallah, J.; Hilaire, L.; Romeo, M.; Le Normand, F.; *J. Electron Spectrosc. Rel. Phenom.* **1995**, *73*, 89.
44. Daucher, A.; Hilaire, L.; Le Normand, F.; Muller, W.; Maire, G.; Vasquez, A.; *Surf. Interface Anal.* **1990**, *16*, 341.
45. Paparazzo, E. *Surf. Sci.* **1990**, *234*, L253.
46. Paparazzo, E.; Ingo, G. M.; Zacchetti, N. J. *J. Vac. Sci. Technol. A*, **1991**, *9*, 1416.
47. Park, W. P.; Ledford, L. S. *Langmuir*, **1996,** *12,* 1794-1799.

CHAPTER 3

THE EFFECT OF DIOL COMPLEXATION AND CALCINATION ATMOSPHERE ON THE STRUCTURE OF $CEO_2/\gamma-AL_2O_3$ CATALYSTS

3.1. Introduction

Anchoring cerium alkoxide species in an organic medium followed by calcination has recently proved to be a reliable preparation technique for supported CeO_2 catalysts [1]. In our previous study of cerium promoted catalysts (chapter 2), we have used simple and hot grafting techniques to prepare a high loadings of small CeO_2 particles supported on a γ-Al_2O_3 catalyst. The method is based on the chemical interaction between a cerium alkoxide compound and the hydroxyl groups from the support surface [2]. Grafting impregnation led, after calcination, to poorly dispersed CeO_2 on alumina. This was attributed partly to the agglomeration of the cerium alkoxide molecules on the support surface through a polymerization process, during impregnation, drying, and calcination. A significant amount of the cerium phase deposited on the alumina surface was found to be in an amorphous state. Increasing the calcination temperature to 800°C enlarged the CeO_2 crystallites deposited on the γ-Al_2O_3 support. Other previous studies have emphasized the strong correlation between cerium surface structure and its promoter and/or catalytic properties [3-10]. This work is a part of our study which investigates new synthetic methods for preparation of catalysts.

In solution, cerium can form complexes with one, two, three, or four bidentate organic ligands. Different discrete structures are obtained by using variable cerium-ligand molar ratios. Sanchez *et al.* [11] have studied the sol-gel chemistry of cerium

isopropoxide using 2,4-pentanedione (acac) as a ligand for the gelation process. Using EXAFS analysis combined with FTIR and Raman spectroscopy they found that cerium isopropoxide is present in the gel as a monomer or dimer alkoxide. Cerium as a metal center can coordinate one, two or three (acac) molecules forming complexes with well defined structure. Based on this idea, it should be possible to make a new complex alkoxide precursor, stable enough to avoid polymerization but reactive to be used for grafting impregnation of a high surface area support, like Al_2O_3, TiO_2 or SiO_2. Diols are organic compounds with two hydroxyl groups in the molecules. These hydroxyl groups can be geminal, or bonded to the same carbon atom (very unstable); vicinal or bonded to two neighboring carbon atoms; or attached to carbon atoms farther apart from each other [12]. Diols are generally viscous liquids which can function as moderate bidentate ligands in complexation reactions due to the nonbonded electrons on the oxygen atoms in their hydroxyl groups [13]. Livage *et al.* [14] explained the chemical modification of metal alkoxides [$(Ti\text{-}OR)_4$] with "acac" in a similar manner, using FTIR and ^{1}H-NMR, respectively. The structural differences are related to the ability of the alkoxide groups to behave as exchange ligands. Another factor which might be considered is the humidity during the preparation of the diol modified cerium alkoxide. It is well known that atmospheric water vapor plays an important role in the gelation process. To avoid gelation before and during impregnation, a dry atmosphere is needed. Extreme conditions like high vacuum or high temperature easily decompose the complexes.

The impregnation process in this case, is similar with that described previously (see chapter 2). The interaction between the precursor and support may imply a reaction

of the cerium alkoxide with the surface hydroxyl groups from the support. This chapter explores the effects of two variables: i) 2,4-pentanediol complexation in the precursor solution used for grafting impregnation; ii) the calcination atmosphere during the thermal treatments on the surface structure of CeO_2 deposited on γ-Al_2O_3 support. Fourier transform infrared spectroscopy (FTIR) and nuclear magnetic resonance (NMR) analysis are used to characterize the molecular structure of the diol modified precursors. X-ray diffraction (XRD) and X-ray photoelectron spectroscopy (XPS) provide information about the bulk and surface structure of the calcined Ce-promoted/Al_2O_3 catalysts prepared using the modified precursors.

3.2 Experimental

Catalyst Preparation. Catalysts were prepared by grafting impregnation of γ-alumina (American Cyanamid, γ-Al_2O_3, surface area = 200m^2/g, pore = 0.6 mL/g) using solutions of modified cerium alkoxide (Cerium Methoxyethoxide solution 18-20% in methoxyethanol, Gelest Inc.) with a diol (2,4-pentanediol 99%, mixture of isomers, Aldrich) at various molar ratios, as precursor. Samples where assigned as D*q*CeAp for precursors and D*q*CeA for catalysts (where q = diol:cerium alkoxide molar ratio). The alumina support was finely ground (<230 mesh) and calcined in air at 500°C for 24 h prior to impregnation. Catalysts derived from pure alkoxide used Ce^{4+}-methoxyethoxide (18-20% alkoxide in methoxyethanol) obtained from Gelest Inc. The modified cerium methoxyethoxide precursors were prepared using 2,4-pentanediol obtained from Aldrich Chemical Company. The cerium content chosen for our catalysts was Ce/Al = 6.0 x 10^{-2}

atomic ratio (or 16.5% CeO_2 by weight), a value close to the monolayer coverage for a γ-Al_2O_3 support. Different diol:cerium alkoxide molar ratios in the precursor solutions were used to prepare the D*q*CeA catalysts, where q = 0, 1, 2, and 3. The catalysts were prepared by wet impregnation of the γ-Al_2O_3 support with the alkoxide and the modified precursor solutions, at room temperature, under inert atmosphere and continuous mixing for 24 h. After impregnation, the catalysts were dried at 120°C for 12 h and calcined 24 hours in air at 500°C and 800°C, respectively.

FTIR Spectroscopy. An FTIR Mattson Inst. Galaxy-3020 was used for infrared analysis of the precursor solutions. Thin precursor films were prepared on KBr and analyzed. IR spectra were acquired with resolution of 2.0 cm^{-1} on a 400-4000cm^{-1} wavenumber range. The spectra are presented in absorption units.

NMR analysis. ^{1}H-NMR spectra for the modified cerium precursors were collected with a Varian Gemini 300 MHz instrument and computer interface. D-Chloroform (singlet at 7.23 ppm) at room temperature was used as reference and solvent. The spectrum of pure 2,4-pentanediol in D-chloroform was acquired as a chemical shift reference in the study of the modified precursors.

X-Ray Diffraction. X-ray powder diffraction patterns were obtained with a Rigaku XRD diffractometer employing Cu Kα radiation (λ = 1.541838 Å). The X-ray was operated at 45 kV and 100 mA. Diffraction patterns were obtained using a scan rate of 0.5 deg/min with DS and SS slits = 1. Powdered samples were mounted on glass slides by pressing the powder into an indentation on one side of the slide. The mean

crystallite size ($\bar{d}$) of the CeO_2 particles was determined from XRD line broadening measurements using the Scherrer equation [15]:

$$\bar{d} = k\lambda / \beta \cos\theta \qquad (1)$$

where λ is the X-ray wavelength, k is the particle shape factor, taken as 0.9, and β is the full width at half maximum (fwhm), in radians, of the CeO_2 <111> line and θ is the diffraction angle. Semiquantitative X-ray diffraction data were obtained by comparing CeO_2 <111> / Al_2O_3 <440> intensity ratios measured for catalyst samples with peak ratios measured for physical mixtures of CeO_2 and γ-Al_2O_3.

XPS Analysis. XPS data were obtained using a Perkin-Elmer Surface Science instrument equipped with a magnesium anode (1253.6 eV) operated at 300W (15 kV, 20 mA) and a 10-360 hemispherical analyzer operated with a pass energy of 50eV. Spectra were collected using a PC137 board interfaced to a Zeos 386SX computer. The instrument typically operates at pressures below 1 x 10^{-8} torr in the analysis chamber. Samples were analyzed as powders dusted onto double-sided sticky tape. Binding energies for the catalyst samples were referenced to the Al 2p peak (74.5 eV). XPS binding energies were measured with a precision of ± 0.2 eV, or better. As reference spectra for cerium oxidation state analysis was used data from Chapter 2, Figure 2.13.

3.3 Results and Discussion

Modified precursors. In solution, different discrete structures can be obtained by using different cerium-ligand molar ratios [2]. Previous studies on cerium alkoxide coordination chemistry used 2,4-pentanedione (*acac*) at different metal to ligand atomic

ration, for metal stabilization by complexation [11,12]. Due to the high reactivity of cerium methoxyethoxide, addition of *acac* solution led instantly to a precipitate. The formation of the precipitate precluded the utilization of acac modified cerium alkoxide solution for catalyst preparation because grafting impregnation requires the use of a homogeneous solution as precursor. A moderate modifier, 2,4-pentanediol (diol), was chosen for this purpose. Adding the diol at different diol:alkoxide molar ratios, homogeneous cerium solutions were obtained. In time, the solutions changed color and formed gels. Aging is an important factor in gels preparation. To avoid the gelation process, the fresh modified solution was used immediately for impregnation. The strongest gelation effect was observed in the case of the diol modified cerium alkoxide at a molar ratio of 3:1. Figure 3.1. shows the ^{1}N-NMR spectrum of the cerium methoxyethoxide solution (a) in comparison with the diol modified alkoxide solutions. From spectrum (a), it can be observed that the resonances corresponding to the -O-CH_3 (δ = 3.28 ppm), -CH_2- (δ = 3.43 ppm) and -O-CH_2- (δ = 3.66 ppm) protons are broad instead of a narrow singlets for (-CH_3) or multiplets (-CH_2-) peaks. This was attributed in the literature [11] to averaging resonances obtained from dynamical chemical exchange of the methoxyethoxide ligand and different ligand groups (terminal or solvated molecules), with the methoxyethanol solvent.

Figure 3.1. (b-d) shows the ^{1}H-NMR for the diol modified cerium alkoxide solutions at different molar ratios [(a)-1:1, (b)-2:1, (c)-3:1]. In these cases, the spectra show characteristic resonances for the protons corresponding to the methoxyethanol from

the cerium solution: a singlet for the $-CH_3$ and a multiplet for the $-CH_2-$ and $-O-CH_2-$ groups.

Table 3.1 ^1H NMR data of *meso*-2,4-pentanediol for modified cerium alkoxide precursors

	Chemical Shift δ [ppm]		
	CH_3-	$-CH_2-$	-CH-
Diol	1.116(d, J=6 Hz, 3H) 1.144(d, J=6 Hz, 3H)	1.464(m, 2H)	3.949(m, 1H) 4.045(m, 1H)
D1CeAp	1.096(d, J=6Hz, 3H) 1.124(d, J=6Hz, 3H)	1.443(m,2H)	3.416(m,1H) 3.629(m, 1H)
D2CeAp	1.123(d, J=6Hz, 3H) 1.159(d, J=6 Hz, 3H)	1.476(m, 2H)	3.441(m, 1H) 3.458(m, 1H)
D3CeAp	1.044(d, J=6Hz, 3H) 1.080(d, J=6Hz, 3H)	1.388(m, 2H)	3.368(m, 1H) 3.584(m, 1H)

Table 3.1 shows the chemical shifts observed for the 2,4-pentanediol protons in the modified solution (D*q*CeAp) in comparison with the pure diol solution [16]. Due to the two asymmetric carbons in positions 2 and 4, of the *meso*-2,4-pentanediol molecules, resonances corresponding to the -CH- protons in the molecules appear at two positions, δ_1 = 3.949 ppm (*m*) and δ_2 = 4.045 ppm (*m*) [17]. Spectra of the diol in the modified precursors exhibits shifting of the free diol resonances due to interactions with cerium ions. For instance considering the peaks characteristic to $-CH_3$ group, δ_{CH3} is 1.096 ppm (1.124 ppm) for the D1CeAp, 1.123 ppm (1.159 ppm) for the D2CeAp and 1.044 ppm

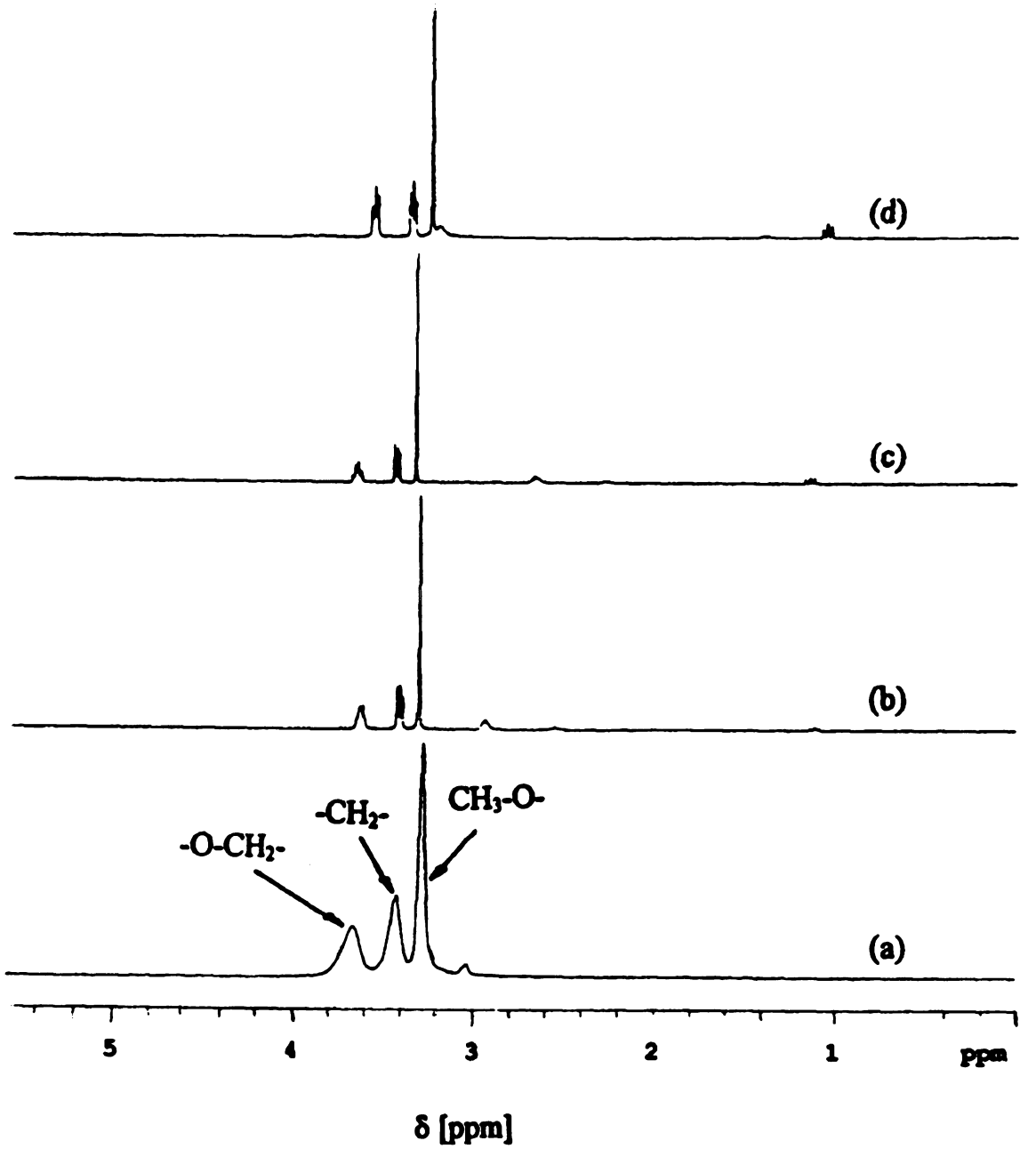

Figure 3.1 ^{1}H NMR spectra of the precursor solutions: a) D0CeAp; b) D1CeAp c) D2CeAp; d) D3CeAp precursors

(1.080 ppm) for D3CeAp compared with the δ_{CH3} = 1.116 ppm (1.144 ppm) for the pure 2,4-pentanediol solution. These new resonance values for the chemical shifts of the diol protons can be assigned to the bonded diol ligands that are coordinated to the cerium atom. The presence of diol in the system may have an effect as moderator, changing the viscosity of the solution by initiating new chemical processes in the system and interfering in the dynamic equilibrium established between the ligands and solvent molecules attached to the cerium atom [11].

Additional information about the complexation and gelation process can be obtained from FTIR analysis. IR spectra of the precursor solutions (DyCeAp) are presented in Figure 3.2. Metal alkoxide exhibits characteristic bands for -C-O- vibrations at ca. 1000 cm^{-1} and M-O- vibration at 600-300 cm^{-1} wavenumber [18]. Cerium isopropoxides exhibit a strong and characteristic absorption band, corresponding to the -C-O- vibration from a -C-O-Ce group, at 980 cm^{-1} [19]. Pure cerium methoxyethoxide IR spectrum shows the analogous band at 910 cm^{-1}. As the diol is added to the alkoxide, a new band appears at 937 cm^{-1} which can be attributed to the new diol -C-O-Ce bend. Other new bands appeared in the IR spectra of the diol modified solution at 1085 cm^{-1}, 1330 cm^{-1} and 1710 cm^{-1}. Absorptions in the region of 1710 cm^{-1} usually indicate carboxylate groups in the system. It is possible that during the complexation and gelation process, carboxylate groups have been formed by ligand decomposition in the cerium alkoxide. With cerium methoxyethoxide molecules 2,4-pentanediol can form a weak complex which inhibits self polymerization of the alkoxide, initially present as a

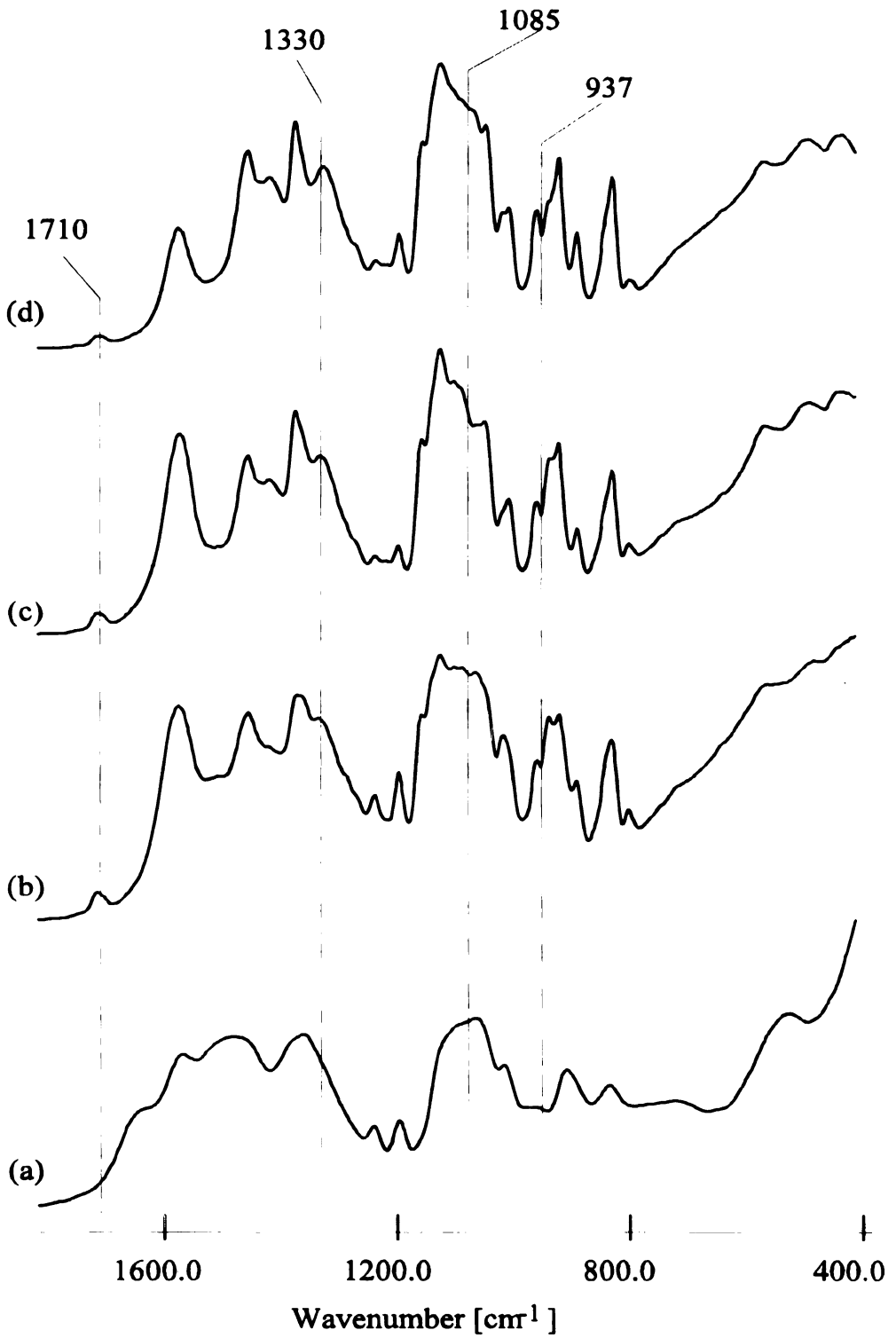

Figure 3.2 FTIR spectra of the precursor solutions: a) D0CeAp; b) D1CeAp; c) D2CeAp; d) D3CeAp precursors

monomer. The diol modified precursor was used for grafting impregnation of the γ-Al_2O_3 support. The impregnation process in this case, is similar with that described previously. The interaction between the precursor and support implies a reaction of the cerium alkoxide with the surface hydroxyl groups from the support. The complex formation determined a change in the precursor structure and the viscosity of the solution used for impregnation modifying the cerium chemical configuration deposited and anchored on the alumina support

Bulk Characterization. Figure 3.3 (b-e) shows the XRD patterns of the D*q*CeA catalysts calcined at 500°C under air, in comparison with the γ-Al_2O_3 support (Figure 3.3 a). The presence of CeO_2 crystalline phase was observed for all catalyst samples. The particle sizes for the crystallites formed on the catalysts' surfaces can be evaluated from line broadening calculations. The results for D*q*CeA catalysts are presented in Table 3.2.

Table 3.2 CeO_2 particle size and crystallinity of D*q*CeA catalysts calcined at 500°C determined from XRD line broadening calculations

Catalyst	CeO_2 Crystalline Phase [%]		Particle Size [nm]	
	500°C	800°C	500°C	800°C
D0CeA	52	100	4.0	9.0
D1CeA	64	100	3.2	3.5
D2CeA	64	77	4.1	11.9
D3CeA	63	96	4.2	15.9

The CeO_2 particle sizes are around 4.0 nm with the exception of the catalyst with

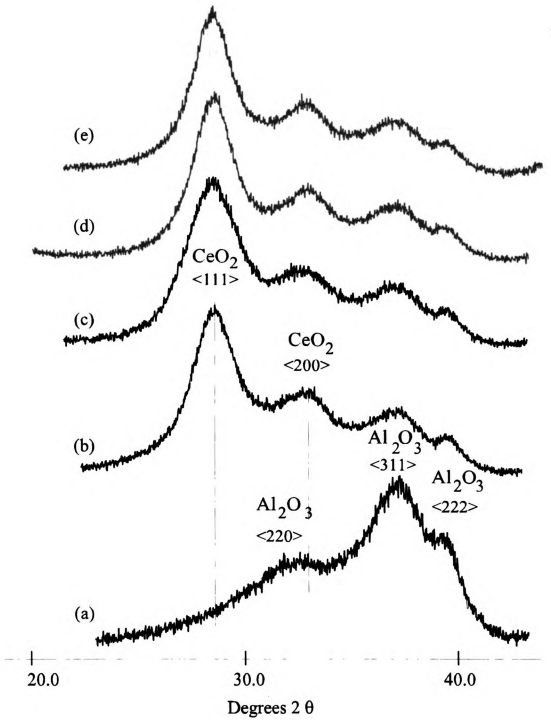

Figure 3.3 XRD patterns for the D*q*CeA catalysts calcined at 500°C: a) Al_2O_3; b) D0CeA; c) D1CeA; d) D2CeA; e) D3CeA catalysts

q = 1, where the particle size is about 3.2 nm. Smaller cerium oxide particles usually correspond to a better dispersion on the high surface area support. This observation can be related with a good interaction of the cerium promoters with the support during grafting impregnation. The CeO_2 crystalline phase present in the DqCeA catalysts calcined at 500°C are around 50% of the total amount of cerium loading added to the catalyst.

The presence of CeO_2 increases the thermal resistance of catalysts used in exothermic catalytic processes [20-22]. To reveal the structural transformation of cerium, the DqCeA catalysts were calcined at high temperature and their structural changes were followed after the thermal treatment. Figure 3.4. (a-d) shows the XRD pattern for the DqCeA catalysts calcined at 800°C. The observed XRD pattern from the figure corresponding to $2\theta = 28.5°$, was assigned to CeO_2 <111> phase. The peak at $2\theta = 32.5°$ is a sample holder artifact. The intense CeO_2 <111> pattern suggests that the cerium in these catalysts is mostly crystalline. The semiquantitative XRD data presented in Table 3.2 indicate a significant amount of amorphous or small crystallites even after calcination at 800°C, in the case of the D2CeA (77%) in comparison with the other catalysts where cerium is present only as CeO_2 crystalline phase. At this moment, there are no clear explanation of this observation for this particular catalyst. However, it is clear that higher temperatures favor crystalline phase formation.

Figure 3.5 (a) presents the XRD pattern for γ-Al_2O_3 support for comparison with

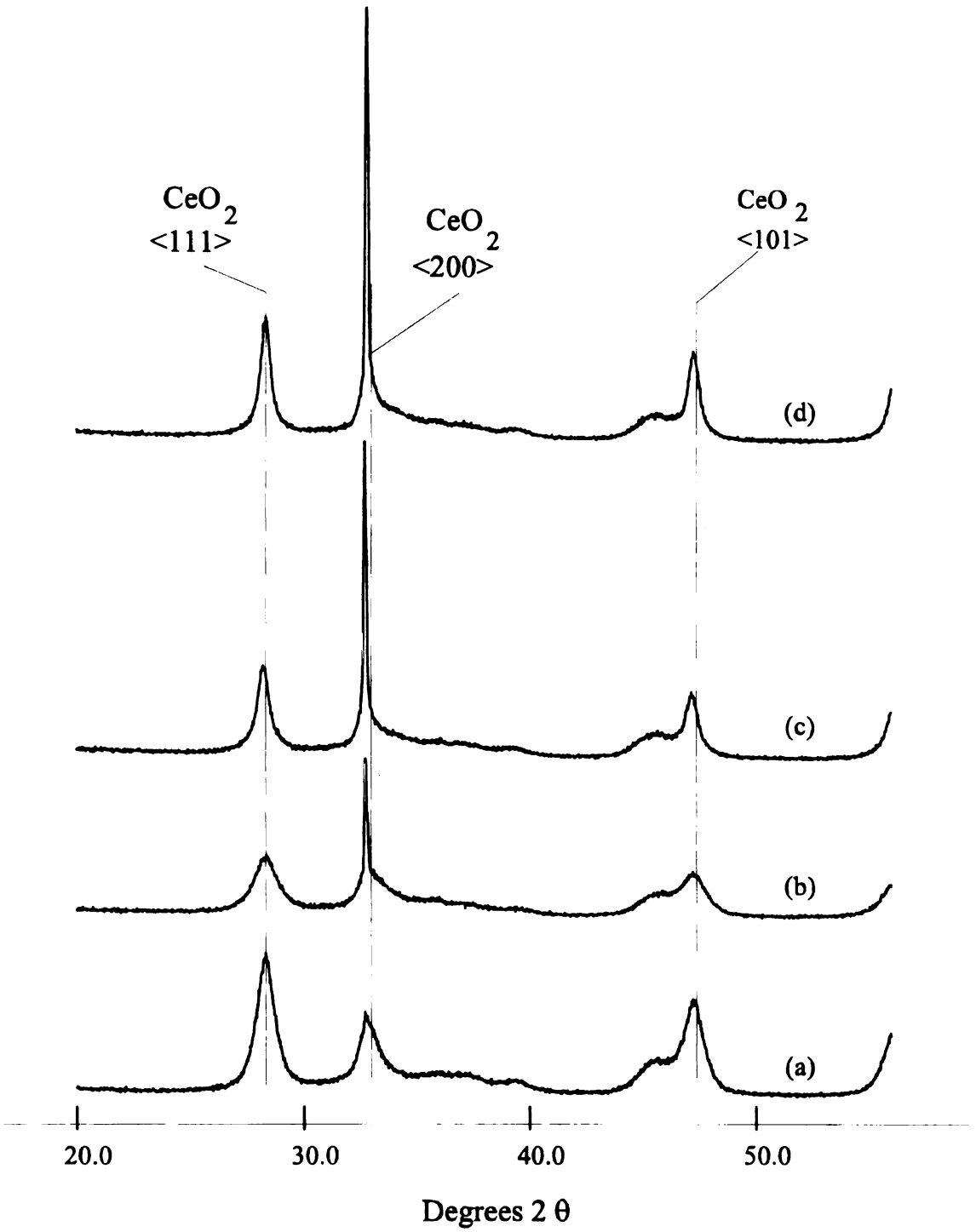

Figure 3.4 XRD patterns for the D*q*CeA catalysts calcined at 800°C: a) D0CeA; b) D1CeA; c) D2CeA; d) D3CeA catalysts

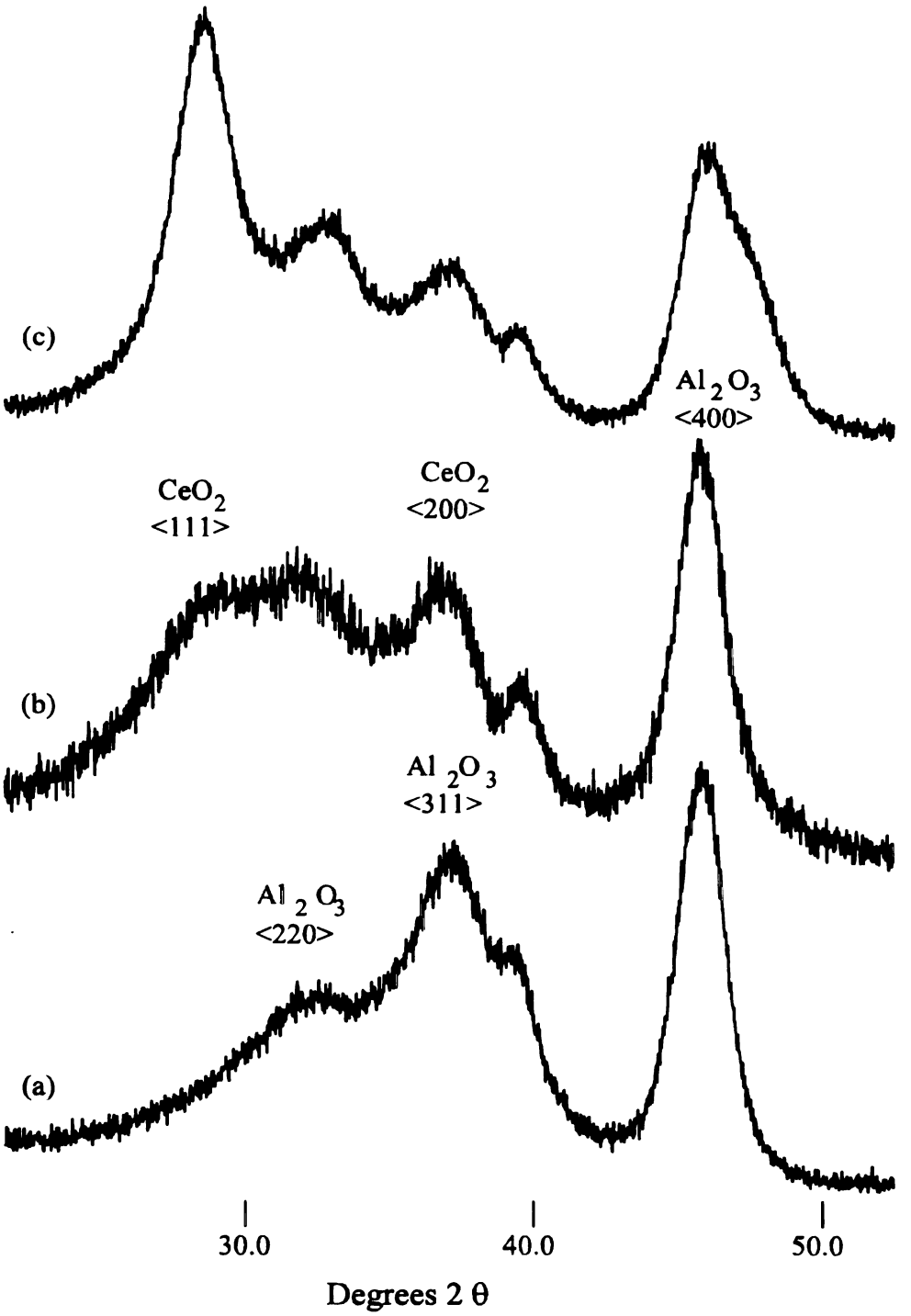

Figure 3.5 XRD patterns for the D0CeA catalysts calcined under different atmosphere: a) pure γ-Al_2O_3; b) D0CeA calcined under hydrogen; c) D0CeA calcined under air

the pattern observed for D0CeA catalysts [spectrum (b)] calcined under a reducing atmosphere (hydrogen flow) and calcined under air [spectrum (c)]. As can be seen in Figure 3.5 (b), the CeO_2 <111> peak almost disappeared when the calcination was performed under a hydrogen flow, at 500°C. This fact can be attributed to the formation of amorphous cerium phases which are not revealed by XRD analysis. It is well known in the literature that surface Ce^{3+}-species are easily oxidized to Ce^{4+}. However, H_2 reduction of supported CeO_2 may disrupt the crystal structure such that room temperature oxidation does not reform the crystal structure. It is unlikely that $Ce^{3+}AlO_3$ is formed at this temperature, these kind of species being observed only after calcination under hydrogen at much higher temperature [23].

Surface Characterization. The XPS spectra for the standard $Ce^{3+}AlO_3$ (a) and $Ce^{4+}O_2$ (b) compounds used as reference are presented in Figure 2.13 (Chapter 2). We have shown that cerium is photoreduced during XPS analysis (Figure 2.14) even in the case of a sample which was previously calcined at very high temperature. The high inhomogeneity of the cerium dispersion on the alumina support, combined with the cerium photoreduction effect observed for amorphous phase precludes quantitative analysis of Ce^{3+}/Ce^{4+} using XPS measurements. Park and Ledford [24] have shown that the amorphous cerium phase is more strongly reduced than crystalline CeO_2 and the fraction of cerium photoreduced decreases with an increase in the CeO_2 crystalline phase. Figure 3.6 (a-d) shows XPS spectra for the D*q*CeA catalysts calcined at 500°C in air, acquired after the same scanning time. This implies that all the catalysts were exposed to

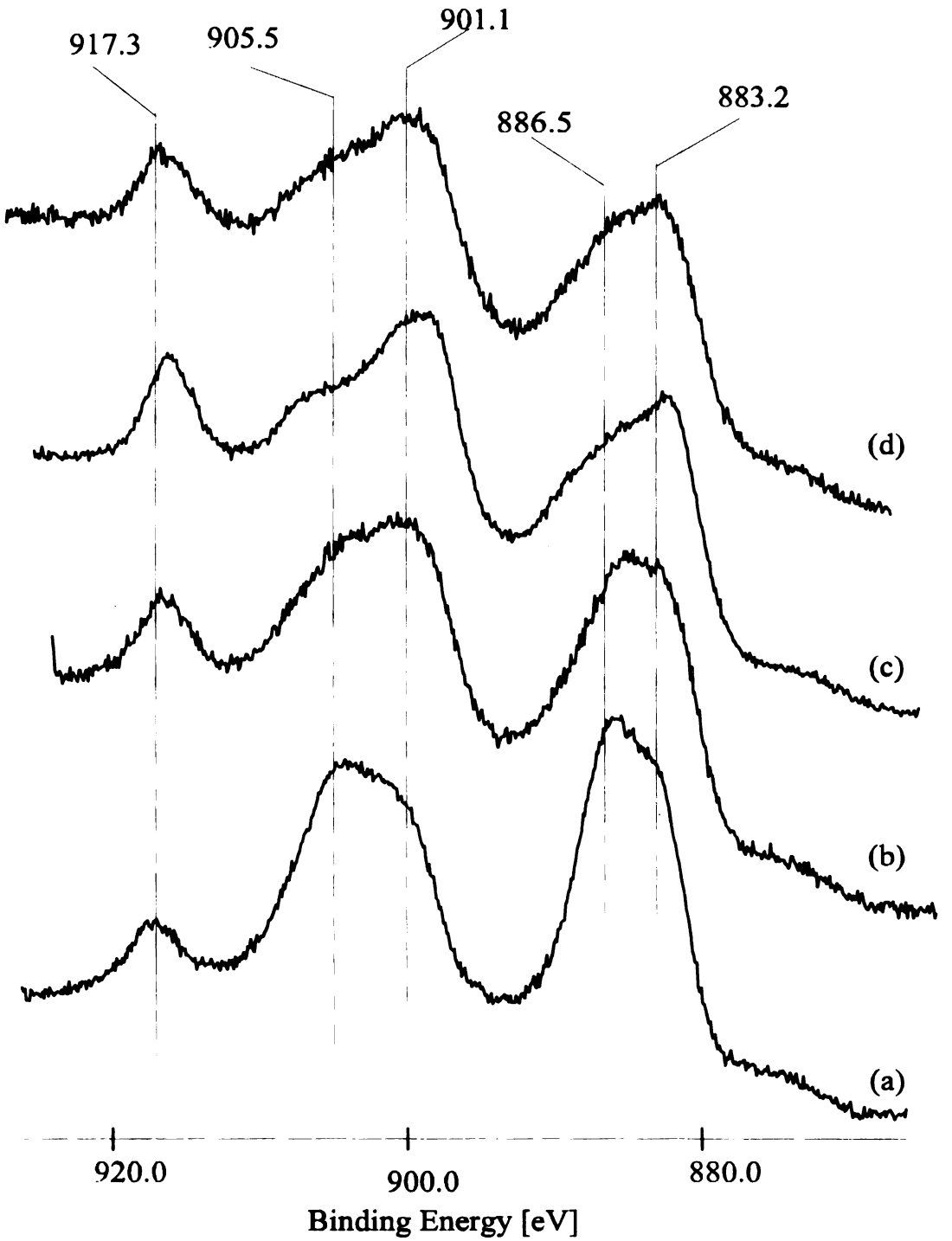

Figure 3.6 XPS spectra of the D*q*CeA catalysts calcined at 500°C: a) D0CeA; b) D1CeA; c) D2CeA; d) D3CeA catalysts

the X-ray for a same period of time. Figure 3.6 (a) shows that the intensity of the Ce v' (u') feature characteristic of Ce^{3+} is dominant in the Ce_{3d} XPS spectrum even if cerium was initially present as Ce^{4+}-phase. The intensity of the Ce v' (u') feature is lower in the case of the D2CeA and D3CeA. In these cases, the Ce^{4+}-features (u", u and v", v) dominates the Ce3d XPS spectrum. The XPS spectrum observed for the D1CeA catalyst is a mixed Ce^{4+}-Ce^{3+}-like shape. Our previous studies (Chapter 2) have indicated that cerium is present as an amorphous phase when the simple grafting method was used for alumina impregnation. Under these conditions, long X-ray exposures should cause cerium to appear strongly reduced in the XPS spectrum. The decreased photoreduction effect observed in the case of the DqCeA catalysts with $q \geq 1$, obtained by impregnation with the diol modified precursors, can be related to the amount of CeO_2 crystalline phase formed. As Table 3.2. shows, the CeO_2 crystallinity increases in the order: D0CeA < D1CeA < D2CeA < D3CeA. This analysis has provided some additional information about the crystallinity of the cerium phase deposited on the alumina support for the DqCeA series of catalysts.

3.4 Conclusions

FTIR and ^{1}H-NMR analysis were used to analyze the molecular structure of the modified cerium alkoxide precursors. Cerium alkoxide can form a weak complex with 2,4-pentanediol, which shows, after aging, gelation behavior. The diol modified cerium alkoxide solution used for grafting impregnation a γ-Al_2O_3 support led to a different cerium structure on the support than in the case of the unmodified cerium alkoxide

precursor. XPS and XRD analysis were used to characterize the cerium oxide on γ-alumina catalysts prepared from modified precursors with different diol:cerium alkoxide molar ratio solutions. The findings for D*q*CeA catalysts indicate that after calcination, different CeO_2 structures were obtained when the diol modified cerium alkoxide precursors was used for alumina impregnation. The diol chelation effect influences the impregnation process with consequences on the surface configuration of the promoter. X-ray photoreduction is an important factor in evaluating the oxidation state of cerium on a catalyst surface; it also offers qualitative information about the presence of amorphous CeO_x. Cerium alkoxide impregnated support calcined under an H_2 atmosphere leads to formation of more amorphous CeO_x phase.

3.5 References

1. Bensalem, A.; Bozon-Verduraz, F.; Delamar, M.; Bugli, G. *Appl. Catal. A*, **1995,** *121*, 81-93.
2. Kifenski, J.; Baiker, A.; Glinski, M.; Dollenmeier, P.; Wokaun, A. *J. Catal.* **1986,** *101*, 1-11.
3. Schaper, H.; Doesburg, E.B.M.; Van Reijen, L.L. *Appl. Catal.* **1983,** *7*, 211-220.
4. Yang, J. K.; Swartz, W. E. *Spectrosc. Lett.* **1984,** *17(6,7)*, 331-334.
5. Yu-Yao, Y. F.; Kummer, J. T. *J. Catal.* **1987,** *106*, 307-312.
6. Oudet, F.; Courtine, P.; Vejux, A. J. *J. Catal.* **1988,** *114*, 112-118.
7. Pembo, J. M.; Lenzi, M.; Lenzi, J.; Lebugle, A. *Surf. Inter. Anal.* **1990,** *15(11)*, 663-668.
8. Koberstein, E. *Unst. St. Proc. Catal.*, Matros, Y. S., Ed., **1990**, 643-647.
9. Chojnacki, T.; Krause, K.; Schmidt, L.D. *J. Catal.* **1991,** *128(1)*, 161-165.
10. Ribot, F.; Sanchez, C.; Livage, J. in *Chemical Processing of Advanced Materials*, **1992,** Wiley, NewYork, 267-275.
11. Sanchez, C; Toledano, P.; Ribot, F. *Mat. Res. Soc. Symp. Proc.* **1990,** *180*, 47-59.
12. Solomons, G. T. W. in *Organic Chemistry - 5-th Edition*, **1992,** Wiley & Sons Inc. New York, p125, p694.
13. Kemp, W. in *Organic Spectroscopy*, Wiley & Sons, New York, 1975.
14. Leaustic, A.; Babonneau, F.; Livage, J. *Chem. Mat.* **1989,** *1(2)*, 240-247.
15. Klug, H. P.; Alexander, L. E. *X-ray Diffraction Procedures for Polycrystalline and Amorphous Materials,* 1-st ed.; **1954,** Wiley: New York.

16. Itoh, O.; Ichikawa, Y.; Katano, H.; Ichikawa, K. *Bull. Chem. Soc. Jpn.* **1976**, *49(5),* 1353-1358.
17. Drago, R. S. in *Physical Methods for Chemists 2-nd Ed.* **1992**, Saunders C.P. Orlando, 211-273.
18. Nakamoto, K. *Infrared and Raman Spectra of Inorganic and Coordinative Compounds*, 3-rd Ed., **1976**, Wiley, Ney York, 230-231.
19. Brown, L. M. Mazdiyasni, K. S. *Inorg. Chem.* **1970**, *9(12)*, 2783-2786.
20. Haneda, M.; Mizushima, T.; Kakuta, N.; Ueno, A.; Sato, Y.; Matsuura, S.; Kasahara, K.; Sato, M. *Bull. Chem. Soc. Jpn.* **1993**, *66*, 1279-1288.
21. Graham, G. W.; Schmitz, P. J.; Usmen, R. K.; McCabe, R. W. *Cat. Lett.* **1993**, *17*, 175-184.
22. Shyu, J. Z.; Weber, W. H.; Gandhi, H. S. *J. Phys. Chem.* **1988**, *92*, 4964-4970.
23. *Powder Diffraction File Search Manual,* I. C. D. D, Swarthmore, **1987**, 57,534.
24. Park, W. P.; Ledford, L. S. *Langmuir*, **1996,** *12,* 1794-1799.

CHAPTER 4

FUTURE WORK

4.1. Preparation of Transition Metal Oxide (Mn, Cr) Catalysts

One of the goals in this study has been to develop new synthetic methods which offer us control over the surface structure of catalysts. This objective is important because it would allow intentional design of catalytic properties into a particular catalys. Differences in promoter and/or supported metal oxide bulk and surface structure would be reflected in the catalysts' stability, activity and selectivity. Preliminary results have indicated that from various preparation techniques, like grafting and pore volume impregnation, Ce/Al-catalysts with different crystallinity and CeO_2 particle size were obtained. We have characterized the structure of the cerium immobilized on the γ-alumina surface. Different activity and selectivity in oxidation reactions are expected due to the various surface structures of the catalysts. In the future work, it is intended to use similar methods of preparation to control the dispersion of multi-component catalysts with transition (Cr, Mn) metal oxide surface active phase and rare earth oxide promoters. Incipient wetness and alkoxide grafting will be used as preparation methods for catalyst impregnation using different Mn (Cr) precursor solutions. Based on previous studies on Mn (Cr) oxide based catalysts [1-6] as well as on the metal alkoxide chemistry of these elements [7,8,9], a new generation of metal oxide supported catalysts could be developed in this work.

4.2 Characterization of mixed metal catalysts

To understand the effects of promoter structure and composition, preparation conditions, active surface phases and catalytic reactions using the new class of chromium and manganese oxide cerium promoted γ-alumina catalysts, several experimental probes will be used. To obtain molecular level information about the preparation mechanism (characterization of the grafting reaction) and the nature of the precursors used for impregnation a detailed FTIR study will be performed. The goal of these IR studies is to look for the existance and possible modes of formation of the chelated structures and consequently to learn about other possible structures of the cerium methoxyethoxide in the precursor solution with different chelating agents (like β-diketonates). With these studies in hand, it would be possible to explain in more detail the nature of the impregnation and understand the "modified grafting" mechanism. It is desirable to obtain information about the relation between the catalysts structure and the reaction mechanism and kinetics using *in-situ* DRIFTS measurements or to use EPR spectroscopy in the case of a radical mechanism. Due to the paramagnetic properties of the cerium and manganese oxides, EPR may be a proper way to analyze their influence on a reaction mechanism.

An important aspect of this research is the characterization of the crystallinity and the dispersion of the active phases (promoter or active component). In order to accurately determine the distribution of the metal oxide phase, the catalysts must be rigorously characterized using bulk and surface analytical techniques. XRD will be used to determine the chemical and physical nature of the species on catalyst surfaces, identifying

the crystalline phases in the catalysts by means of lattice structural parameters and obtaining data regarding the particle size.

Additional information about the structure morphology and crystallography of the supported species can be provided by electron microscopy. The method can reveal information about the composition and internal structure of the particle. Transmission electron microscopy (TEM) will be used in this work to provide a second measure of the crystalline phase(s) and to characterize the amorphous or the highly dispersed surface phases that can not be detected by XRD. These methods can provide more information about the dispersion of the different species from the catalysts surface.

XPS can be used to obtain information about chemical state of supported phases in the top 3 nm from the catalysts surface (approximately 10 atomic layers). However, in many cases one is interested in the structure of the first atomic layer of the catalyst surface. For example, several of the grafted catalysts to be prepared for this study involve the formation of phases that are expected to be only 0.5-1.0 nm thick [8]. XPS can follow chemical changes in the chemical nature of these surface phases but changes in particle geometry may be difficult to discern. Ion scattering spectroscopy (ISS) can be used to determine the composition and morphology of these monolayer systems[1]. DRIFTS analysis may complete the system characterization by giving information about the catalytic properties of the new catalysts. It offers the advantage that it is an excellent method for analyzing powder materials avoiding the tedious preparation of wafers used in

[1]The ISS method uses ions as input "particles", with energies of 0.5-20 keV; it measures the energy of the scattered ions as output "particles" after binary collisions. The method provides information on the first layer from the surface monolayer (adsorbates on single-crystal substrate) [10]

common IR analysis. The analysis is very sensitive being able to detect adsorbed molecules at minimum 10^{-5} of the monolayer coverage. Quantitative possibilities and *in-situ* capabilities of DRIFTS makes the method very attractive for the purpose of this project (kinetics and mechanistic measurements) [11].

4.3 Mechanism and kinetics of emission control reactions

In this part of the research, a transition metal oxide (Cr and Mn) base on a Ce(La) promoted γ-alumina catalyst will be designed and the system's catalytic activity, selectivity and stability will be probed in total oxidation reaction for CO, CH_4 and $CHCl_3$ streams as well as in ethylbenzene oxydehydrogenation reaction. The effect of the catalysts structure on catalytic properties will be carefully studied. Activity data (rate constant determination and Arrhenius plots for activation energy) will be collected at low conversion to limit heat and mass transfer effects on the rate measurements. This will allow the determination of structure-activity relationships that could lead to more advanced catalysts. In addition, the best catalysts will be studied at high conversion to simulate actual industrial operating conditions and to observe the reaction mechanisms, lifetimes of the catalysts and deactivation processes. With its excellent qualitative and quantitative possibilities, DRIFTS analysis will be used for evaluation of the mechanism and kinetics for the studied reaction. IR analysis will be performed in a cell capable of obtaining temperature between 100K and 773K in a variety of reactive atmospheres [12]. This will allow measurements of adsorbed species to be performed *in-situ*. DRIFTS can

readily detect changes in the surface concentrations of CO or hydrocarbons fragments adsorbed on a catalyst surface close to 10^{-5} monolayer coverage [11, 13].

It is intended to use the power of surface analytical techniques to determine the nature of active sites and the mechanism of a probe process which can simulate a real reaction used in emission control processes. An XPS instrument is equipped with an *in-situ* reactor that can perform reactions at temperature up to 773K at atmospheric pressure and transfer the reacted sample to the ultrahigh vacuum chamber without exposure to the air. This will allow us to perform XPS analysis of the activated catalyst surface and reveal the changes of the surface configuration after reactant adsorption. Chromium and manganese are elements very labile to oxidation state changes. *In-situ* XPS measurements may be crucial for identifying the active sites from these types of catalysts. Oxidation-reduction studies using these cells may give us additional information about the flexibility of oxidation state changes of the catalyst surface and the consequences on the surface configuration. The great interest for the study of a Cr(Mn) oxide based catalysts indicates their importance in industry and recently in emission control processes. Despite the considerable amount of effort devoted to the study of Cr(Mn) catalyst, the active sites of these catalysts, the role of promoters, the mixed effect of single oxides, and the nature of any surface phases is still little known. More detailed work, based on new catalyst preparation methods and advanced surface studies using the new and sophisticated surface analysis techniques, is necessary for a better understanding of these processes. These studies can be applied for industrial environmental protection technologies and selective oxydehydrogenation reactions.

4.4 References

1. Ivanova, A. S.; Dzisco, V. A.; Moroz, E. M.; Nosckova, S. P. *Kinet. Katal.* **1986**, *27(2),* 428-434.
2. Robinsin, E. *Rev. Port. Quin.* **1977,** *19(1-4),* 103-106.
3. Johnson, A. J.; Meyer, F. G.; Hunter, D. I.; Lombardi, E. F. *Incineration of polychlorinated Biphenyl using a Fluidized Bed Incineration, Rockwell International, 18-th Sep.*, RFP-3271, **1981**.
4. Bedford, R. E.; LaBarge, J. *Base Metal Automotive Exhaust Catalysts with Improved Activity and Stability and Method of making the Catalysts*, US 5063193 A 5 Nov. **1991**, 1-9.
5. Prasad, R.; Kennedy, L. A.; Ruckenstein, E. *Combust. Sci. Technol.* **1980**, *22*, 271-275.
6. Agarwal, S. K.; Spivey, J. J.; Butt, J. B. *Appl. Catal*, **1992**, *81*, 259-263.
7. Weldon, J.; Senkan, S. M. *Combust. Sci. Technol.* **1986**, *47*, 229-234.
8. Ribot, F.; Sanchez, C.; Livage, J. *Chemical Processing of Advanced Materials*, **1992**, Wiley, NewYork, 267.
9. Sanchez, C; Toledano, P.; Ribot, F. *Mat. Res. Soc. Symp. Proc.* **1990**, *180*, 47.
10. Hercules, D. M. *J. Chem. Ed.* **1984**, *61* 592.
11. Craciun, R.; Dulamita, N.; Miller, D. J.; Kackson, J. E. submitted and accepted to *Progress in Catalysis*, **1996**.
12. Hamadeh, I. M.; King, D.; Griffiths, P. R. *J. Catal.* **1984**, *88*, 264-72.
13. Fraser, D. J. J.; Griffiths, P. R. *Appl. Spectrosc.* **1990**, *44*, 193-199.